Universität Hamburg

Synchrotron Research Institute

YEREVAN STATE UNIVERSITY

German-Armenian Joint Practical Course
on Accelerator Physics

Vibrating wire monitors and beam profile measurements

Supervisor: Dr. Suren Arutunian

Federal Foreign Office

Supported by the German Federal Foreign Office under Kapitel 0504, Titel 68713

YEREVAN, ARMENIA
2019

Contents

Abstract

We present a practical course which aims at profiling the beam of the AREAL accelerator (CANDLE SRI), using the vibrating wire method. The course includes a detailed overview of existing beam profiling methods. The specific parameters and usage features of different technics are presented.

The monitors developed by our group use a vibrating wire as a sensitive element. The exact measurements of the frequency of the vibrating wire exposed to the beam provides information on local density distribution of the particles in the beam. The proposed method has high sensitivity to the value of local flux of particles and can be a good alternative to other existing methods of beam profile measurement, especially in the beam halo.

1. Bam profile measurement in accelerators

Measurement of beam profiles in accelerators is one of the important tasks of accelerator diagnostics. As in the other areas of diagnostics, a number of methods are discussed here, based on accelerator beam parameters, as well as on the assigned tasks. Especially, it is important to note a significant difference in diagnostics during the accelerator construction and commissioning process and diagnostics during accelerator operation. In the first case, as a rule, the task of steering the beam constitutes a certain stage in the acceleration process. The large number of bending, focusing and correction magnets give rise to the need for many profile measurements [1]. At this stage, methods that completely destroy the beam can be used.

In contrast, in the second case, it is required to apply methods of minimally influencing the beam and providing online information on the quality of the beam. For example, it is important to control the beam width, position and distribution in transversal directions. Another important parameter is the speed of the measurement, which is also determined by the tasks. Measuring the cross-sectional profile of an individual bunch and the average of a beam are very different tasks requiring completely different techniques. The type of accelerator also determines the difference in diagnostic methods. Therefore, the methods permissible in single-pass

linear accelerators would destroy the beam in accelerator types with closed multiturn cycles. The current and energy of the particles are also essential parameters, which dictate the choice of certain measurement schemes. Accelerators with very high current dictate specific methods of diagnostics. For example, in the International Fusion Materials Irradiation Facility project (also known as IFMIF), which is aimed to fully qualify materials for fusion reactor, the current of the two 40 MeV deuterons beams reaches 125 mA. This makes difficult the installation of certain measurement devices, and diagnostics can be made exclusively by contactless methods or only at the periphery of the beam[1].

In beam profiling, the level of requirements for profile detailing is important. In some cases, information on the distribution of particles only in the central region of the beam is sufficient. For the Gaussian particle distribution model, this corresponds to a 3-4 sigma (core) profiling. In other cases, it is necessary to provide a larger dynamic range, which allows measurement of the profile outside the central region in a so-called halo region. This problem is especially relevant for accelerators with a long beam lifetime, where particle losses occur through particle leaks through the halo region.

In this review, we present the main methods for measuring beam profiles in accelerators.

Beam profile

Transverse beam profiles express the particles distribution in a beam as a function of the transverse position, thus we have a horizontal profile expressing the number of particles at different horizontal positions, and we have a vertical profile expressing the number of particles at different vertical positions [2].

As a rule, the aim of the transversal beam profile measurement in the beam core is to determine the transverse shape of the beam up to about 3 to 4 sigma. Therefore, a dynamic range of 10^3 to 10^4 is sufficient for a single measurement [3].

All profile measurement methods can be divided into two classes: 1D and 2D [2].

[1]IFMIF-EVEDA, IN-IF-ACXX-0xx, Beam Instrumentation Preliminary Design Review, June 2010, Beam Instrumentation, IFMIF PDR.pdf.

In the one-dimensional sampling the following instruments are traditionally used:

- Wire scanners
- Wire grids
- Rest gas ionization monitors
- Laser wire scanners

In the two-dimensional sampling, techniques based on screens and radiators are usually used. In circular machines, synchrotron radiation is often applied as a 2D replica of the beam profile. Taking advantage of the rapid development and the huge market for commercially available optical sensors, in the past years optical measuring techniques took on a greater significance. Nowadays area scan CCD or CMOS sensors are widely used in beam diagnostics because they provide the full 2D information about the transverse particle beam distribution, allowing in principle to investigate shot-to-shot profile fluctuations at moderate repetition rates.

In general, there are two types of measurement methods: Nearly non-destructive devices and destructive devices [2, 4]:

- nearly non-destructive devices, such as harps, profile grids, SEM grids, residual gas ionization monitors, viewing screens (holds only if the penetration depth is large in comparison to the screen thickness), and wire scanners,
- destructive devices, such as segmented Faraday cups, Faraday cups combined with scanning slits, and sandwich detectors used for emittance measurements

It should be stressed that there is an important difference between beam tails and beam haloes: tails are deviants from the expected beam profile in the order of percent or per mille while haloes are much smaller in intensity. Fig. 1 shows two examples of beam tails and beam halo to visualize this difference. Since profile measurements are often questioned at the level of a few percent, e.g., by instrumental uncertainties, the difficulty is easily seen in making halo measurements already at the level of 10^{-4} and beyond [4, 5]

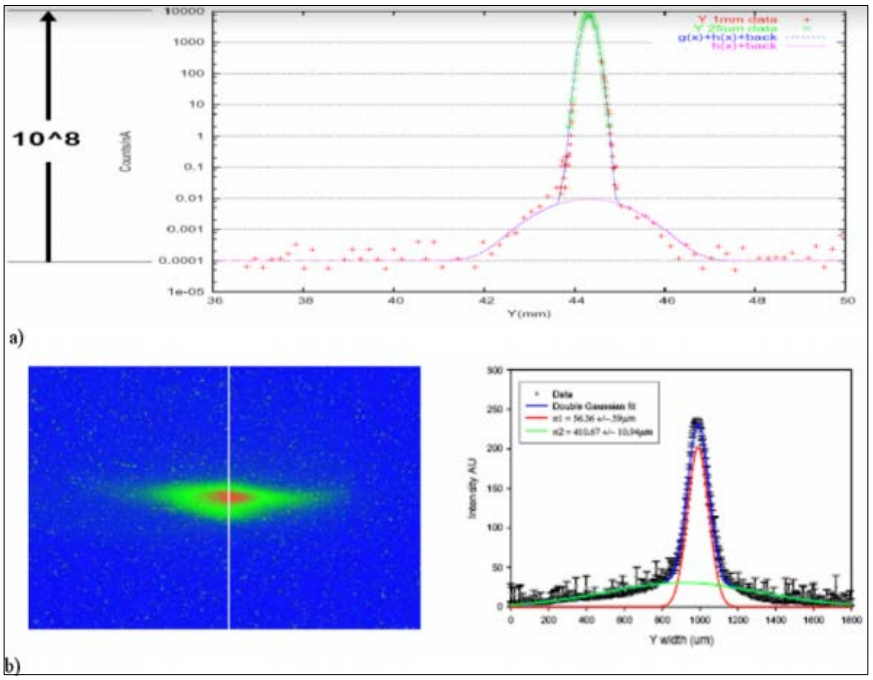

Fig. 1. (a) Beam halo determination with a dynamic range of 10^8; (b) The green curve is a halo and not a tail (which is the low amplitude part of the red curve) [5]. Note the logarithmic vertical scale in both diagrams.

Screen

The most direct way of beam observation is the light emitted from a scintillation screen, monitored by a commercial video or CCD camera, see e.g. [1] for an overview (see also [1],[2]). These devices are installed in nearly all accelerators from the source up to the target and are schematically shown in Fig. 2 together with a realization where the pneumatic feed-through is mounted on a Ø200 mm flange.

[1] R. Jung, G. Ferioli, S. Hutchins, SINGLE PASS OPTICAL PROFILE MONITORING, Proc. Diag. Instrum. Part. Acc. Conf., DIPAC03, Mainz, 2003, p. 10-14.

[2] P. Forck, C.A. Andre, F. Becker, R. Haseitl, A. Reiter, B. Walasek-Höhne, W. Ensinger, K. Renuka, Scintillation Screen Investigations for High Energy Heavy Ion Beams at GSI, Proc. Diag. Instrum. Part. Acc. Conf. DIPAC11, Hamburg, 2011, pp. 170-173.

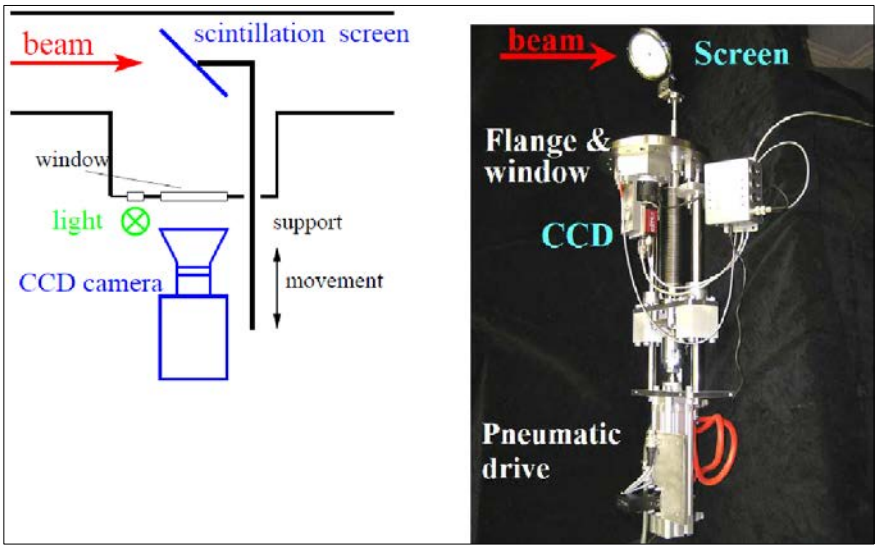

Fig. 2. Layout of an intercepting scintillator screen is shown on the left side. On the right side there is a photo from a P43 phosphor scintillation screen of Ø70 mm and the CCD camera are mounted on a Ø200 mm flange with pneumatic feed-through [1].

When a charged particle penetrates a material, the energy loss can be transformed to fluorescence light. The important properties of such a scintillator are [1]:

- High light output matched to the optical system of the CCD camera in the optical wavelength range (450 nm < λ < 700 nm).
- High dynamic range, i.e., a good linearity between the incident particle flux and the light output. In particular, a possible saturation of the light gives rise to a deformation of the recorded profile.
- No absorption of the emitted light to prevent artificial broadening by the stray light inside the material.
- Fast decay time, to enable the observation of possible variations of the beam size.
- Good mechanical properties for producing up to Ø100 mm large screens.
- Radiation hardness to prevent permanent damage.

For high intensity beams, one has to make sure that the material is not destroyed by the power absorption. A disadvantage of the screen is related to the interception. The used material is so thick (several mm) that it causes a large energy loss, so it can never be used for the diagnostics of a circulating beam inside a synchrotron. The screen is observed with a CCD camera. In older applications with video (i.e. analogue output), the digitalization is done with a frame grabber. A modern approach

uses a digital link, with a digital data transfer of the CCD pixel values. In most cases, fiber optic links are used to get fast data rates and larger cable length without signal degeneration (see e.g.[1],[2]). A problem is the radiation sensitivity of the CCD sensor and the digital equipment. At high levels of radiation, the old-fashioned analogue VIDICON cameras are used.

Secondary emission monitor (SEM) grid

When particles hit a surface, secondary electrons are liberated [1]. For the profile determination, individual wires or ribbons interact with the beam; this is called a Secondary Electron Emission grid or a harp. Each of the wires has an individual current-to-voltage amplifier. This is an electronic alternative to a scintillation screen with a much higher dynamic range i.e., the ratio of minimal to maximal detectable current is orders of magnitude larger.

For low energies at proton or heavy ion LINACs the particles are stopped in the material or undergo a significant energy loss. The ratio diameter-to-spacing of the wires determines the attenuation of the beam current (and of course also the signal strength on the individual wires). Typically, only 10 % of the beam area is covered by the wires and, in this sense, the profile measurement is nearly non-destructive. For energies above 1 GeV/u, the relative energy loss is negligible at single-pass accelerators and large size ribbons are used.

The SEM electronics have to be installed close to the accelerator hardware. With a multiplexer, the analog values are transported to an ADC located outside of the accelerator tunnel. Readout of a full SEM-grid usually takes less than a ms, which is typical for the use of pulsed or dc beams.

An interesting application for a profile measurement is the control of the injection into a synchrotron. If the orientation of the injected beam emittance is wrong due to a

---

[1] A. Peters P. Forck, A. Weiss, A. Bank, TRANSVERSE BEAM PROFILE MEASUREMENTS USING OPTICAL METHODS, Proc. Diag. Instrum. Part. Acc. Conf. DIPAC01, Grenoble, 2001, pp.123-125.

[2] R. Haseitl, C. Andre, F. Becker, P. Forck, BEAMVIEW - A DATA ACQUISITION SYSTEM FOR OPTICAL BEAM INSTRUMENTATION, Proc. PCs at Part. Acc. Conf. PCaPAC2008, Ljubljana, 2008, pp. 180-182.

misaligned focusing, beam storage may still be possible, but can be improved with the help of diagnostics.

The SEM signal is typically used with low-energy beams as in this case no energetic secondary particles are generated; this signal tends to be quite small and requires care in the acquisition. A serious problem with the detection of secondary emission is the fact that when the wire is heated above 1000 ^{0}C by the beam, it starts emitting electrons by thermionic emission perturbing the measurement of the SEM current [2].

Wire scanner

Instead of using several wires with individual, expensive electronics, a single wire can be swept through the beam [1] (see also[1]). The advantage is that the resolution is not limited by the wire spacing and therefore this technique is often used at electron accelerators with beam sizes in the sub-mm range. It can also be applied in proton synchrotrons due to the small amount of intercepting matter.

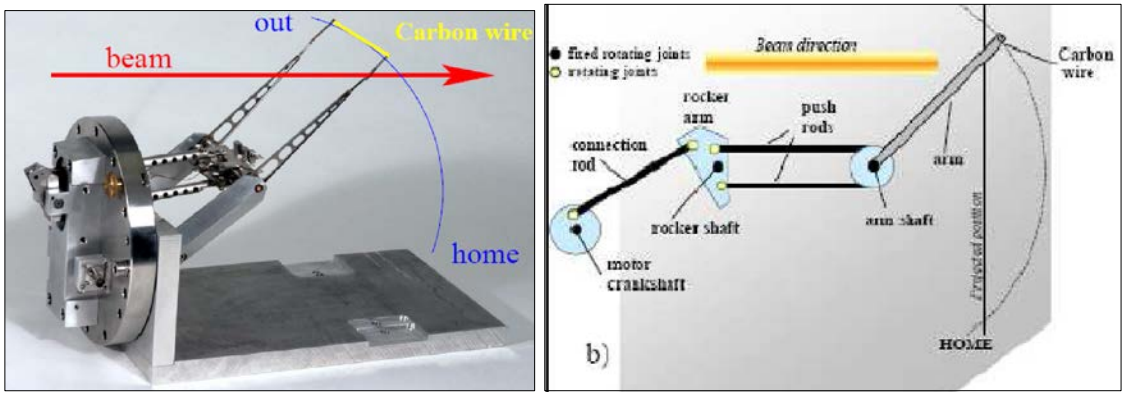

(a) (b)

Fig. 3. (a) Pendulum scanner or «flying wire» used at the CERN synchrotron [1, 6]. (b) kinematic scheme of the scanner [2].

The signal from high-energy secondary particles is typically large due to the high gain of the scintillator/phototube detector. On the other hand, beam losses can pollute the signal and, more importantly, due to the geometry of the detector and of the beam line, the signal induced in the detector may depend on the position of the wire and direction of the particles, introducing distortions and aberrations in the profiles [2].

[1] M. Plum, Interceptive Beam Diagnostics—Signal Creation and Materials Interactions, Beam Instrum. Workshop, Knoxville, 2004, AIP Conf. Proc. 732, p. 23.

Scanning velocities up to 10 m/s can be achieved with a special pneumatic mechanism. Sometimes this setup is also called «flying wire» (see e.g. Fig. 3). As the wire material, carbon or SiC is used due to its low weight and low nuclear charge Z, resulting in a low energy deposition in the wire [1]. These materials can withstand high temperatures without melting. The thickness can be down to 10 µm. But due to the scanned single wire and the high speed of the particles the profile is not taken at a single instant, even with high scanning velocity. Therefore, only the steady state distribution can be probed. For the display of the profile, the position of the wire, determined by the position encoder, is plotted on the horizontal axis. The beam signal for the vertical axis can be deduced from the current given by the emitted secondary electrons, like for a SEM-grid. This is done in particular for low energy protons and heavy ions. In most cases for beam energies larger than 150 MeV/u for ions (the threshold for π-meson production) or 10 MeV for electrons the signal is deduced by monitoring the secondary particles outside of the beam pipe (see Fig. 4). These secondary particles might be hadrons created by the nuclear interaction of the proton or heavy ion projectiles and the wire, having enough kinetic energy to leave the vacuum chamber. For the case of electron accelerators, the secondary particles are mainly Bremsstrahlung-photons. The detector is just a type of well suited beam loss monitor, e.g. a scintillator installed several meters away. The count-rate is plotted as a function of the wire position as a precise representation of the beam profile.

Silicon Carbide (SiC) coated carbon wires with diameters of 142 µm are used for the measuring wires in [7] (scanning wire monitors of ISIS Neutron and Muon Source, based at the Rutherford Appleton Laboratory). This material was noted as an ideal choice due to its rigidity and high emissivity, meaning it does not suffer from excess heating whilst intercepting the beam.

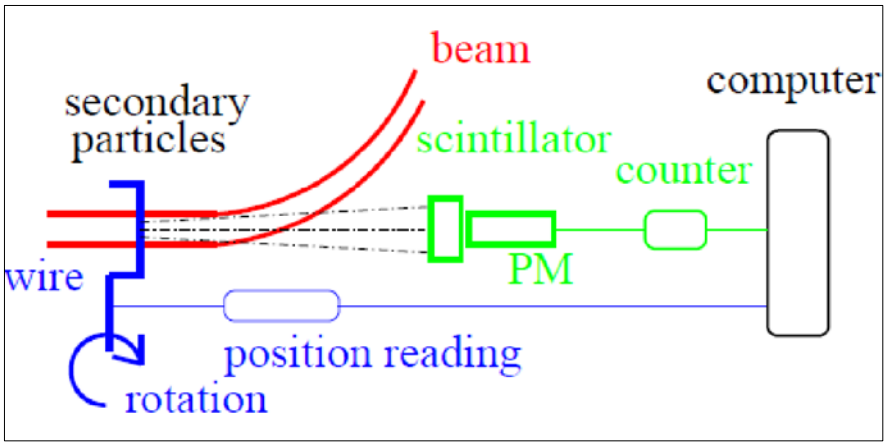

Fig. 4. Scheme of a wire scanner using the production of secondary particles as the signal source [1].

A comparison of the wire scanner and the SEM-grid shows the advantages and disadvantages of both types:

- With a SEM-grid the beam intensity is sampled concurrently, whereas a moving wire samples the parts of the profile at different locations at different times. Therefore, variations of the beam intensity in time will be mixed with transverse intensity variations using a scanning device.
- In case of pulsed beams further complications may arise based on the need for exact synchronization, which can be easily solved in case of SEM-grid application.
- The resolution of a SEM-grid is fixed by the wire spacing (typically 1 mm), while a wire scanner can have much higher resolution, down to 10 µm, due to its constant movement. For high resolution, mechanical vibration has to be avoided.
- The electronics for data acquisition is cheaper for a scanning system. A SEM-grid requires one channel per wire.
- For the cost of the mechanics it is vice versa: The precise vacuum actuator for the scanner is more expensive than the pneumatic feed-trough needed for a SEM-grid.

The superconducting CW LINAC, presently being commissioned at TRIUMF, will accelerate up to 10 mA of electrons to the energy of 30 – 50 MeV. Thus, average beam powers up to 0.5 MW are eventually expected. To support high beam power operation modes, a Fast Wire Scanner (FWS) capable of velocities up to 3 m/s over a 70 mm range was developed [8]. A stepper motor driven helical cam allows for a

long stroke enabling two orthogonal wires to scan both axes in one scan. The radiation produced when the wires pass through the beam is detected by a BGO scintillator coupled to a photomultiplier (PMT), while the wire position is measured with a precision linear potentiometer.

Ref. [9] describes a new approach to wire scanners design based on nanofabrication technologies. This approach opens up new possibilities in term of wires shape, size, material and thickness with potential for even higher resolution and increased flexibility for instrumentation designers. The device, fabrication process and report measurement performed on the FERMI FEL electron beam are presented. An interesting investigation aimed to fabricate micrometer sizes wire scanners is reported in [8].

In [1] is noted that compared to view-screens monitor the beam profile wire scanners are normally immune to non-linear effects of the signal response and can perform high resolution measurements which ultimately depends on the wire diameter and scanning speed.

Wire scanners are considered as a good instrument especially for beam halo measurement [2] (see also [2], [3])

---

[1] G.L. Orlandi, A. Alarcon, S. Borrelli, A. Gobbo, P. Heimgartner, R. Ischebeck, D. Llorente, F. Loehl, C. Ozkan Loch, P. Pollet, B. Rippstein, V. Schlott, First experimental results of the commissioning of the swiss FEL wire-scanners, 6th International Beam Instrumentation Conference IBIC2017, Ljubljana, Slovenia, 2017 pp 388-392.

[2] K. Wittenburg, DESY, MDI, Halo Monitoring: Very High Dynamic Beam Profile Measurements, Halo introduction.pptx, URL: https://www.google.com/url?sa=t&rct=j&q=&esrc=s&source=web&cd=1&cad=rja&uact=8&ved=2ahUKEwiN2_Dl6ubiAhUPcZoKHWYNARAQFjAAegQIABAC&url=https%3A%2F%2Fportal.slac.stanford.edu%2Fsites%2Fconf_public%2Fbhm_2014%2FPresentations%2FWittenburg%2C%2520Halo%2520introduction.pptx&usg=AOvVaw0Q9LzW-s1CN7vbb5TiF1Gh

[3] K. Wittenburg, Beam halo and bunch purity monitoring, URL: https://cas.web.cern.ch/sites/cas.web.../wittenburg-halo2.pdf.

Multi-wire proportional chamber MWPC

For slowly extracted beams from a synchrotron, the current is much too low to be measured by a SEM-grid. One can use the amplification of electrons in a gas as done in a Multi-Wire Proportional Chamber MWPC. For the operation principle, see e.g. [1, 10]. The primary particles traverse a gas (like 90 % Ar mixed with 10 % CH_4 or CO_2), creating secondary electrons. A MWPC consists of a grid held at a high voltage, typically several kV, and a grounded grid, which is read by a charge-sensitive pre-amplifier, like for SEM-grids. The distance between the anode and the cathode plane is typically 1 cm and the spacing of the wires is about 1 mm. The principle is shown in Fig. 5. After reaching a threshold, the energy of the electrons accelerated toward the wires is high enough to knock out additional electrons from the gas atom/molecules. This gives rise to an avalanche, which results in a $\sim 10^4$ amplification of the number of electrons. This amplification inside the detector volume is nearly noise free due to the, electrically spoken, high source impedance of the free charge carriers. The resulting low noise could not be achieved by an electric amplifier due to its thermal noise. The following electronics (further amplifier and ADC) and the way of displaying is comparable to the procedure for SEM-grids.

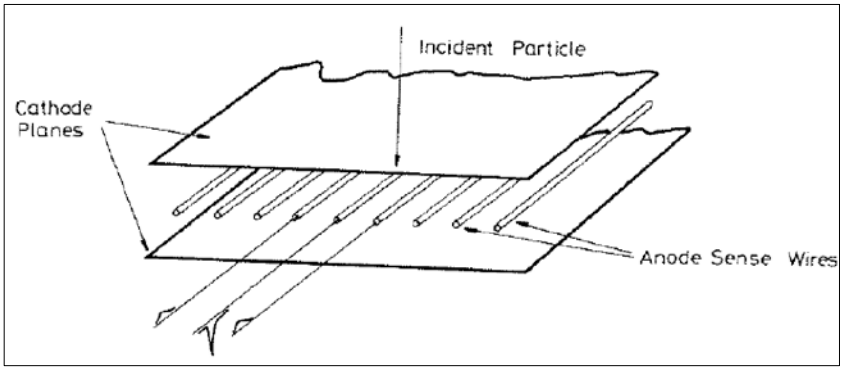

Fig. 5. The scheme of a MWPC for one plane showing the type of signal generating by a particle interaction [1].

Residual gas monitor

A frequently used non-destructive method for the profile determination is the Residual Gas Monitor RGM; it is sometimes also called Ionization Profile Monitor IPM [1]. The IPM is based on the interaction of the beam and the rest gas present in the vacuum chamber; even in the best vacuum there are still 10^{13} ions/cm^3 [2]. Such

monitors are installed in nearly every proton/heavy ion synchrotron for the detection of beam sizes between some mm and several cm. For electron synchrotrons, they are not used so often, due to the smaller electron beam dimensions. The idea is to detect the ionized products from a collision of the beam particles with the residual gas atoms or molecules present in the vacuum pipe. Typical pressures for LINACs and transfer lines are in the range of 10^{-8}–10^{-6} mbar containing mainly N_2 and O_2 and for synchrotrons 10^{-11}–10^{-9} mbar containing mainly H_2. The different compositions are due to the different vacuum pumps used. A scheme for such a monitor is shown in Fig. 6. Due to electronic stopping, electrons are liberated and electron-ion pairs are generated. An estimation of the signal strength can be obtained by the Bethe-Bloch formula.

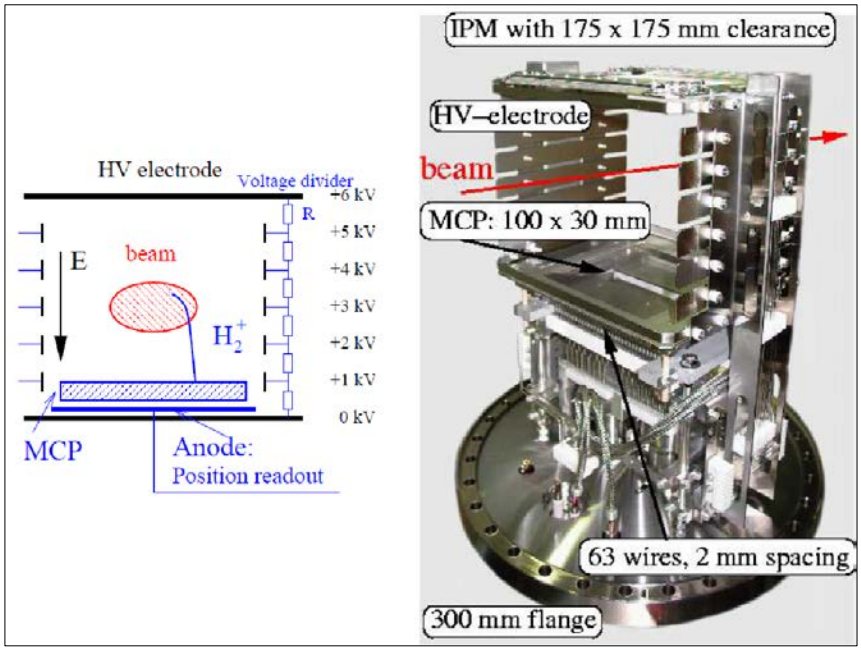

Fig. 6. Left: Scheme of a residual gas monitor for the horizontal profile determination. Right: The large aperture residual gas monitor installed at the GSI synchrotron for the horizontal direction. The clearance is 175×175 mm^2. The monitor is mounted on a Ø 300 mm flange. The read-out behind the MCP (bottom) is done with an array of 63 wires with 2 mm spacing [1].

The reconstruction technique of a two-dimensional beam density distribution through a residual gas ionization was initially proposed in the Kurchatov institute [11, 12]. The

concept of Beam Cross-Section Monitors (BCSMs) based on ion components of a residual gas ionization is presented in Fig. 7 (see also[1]).

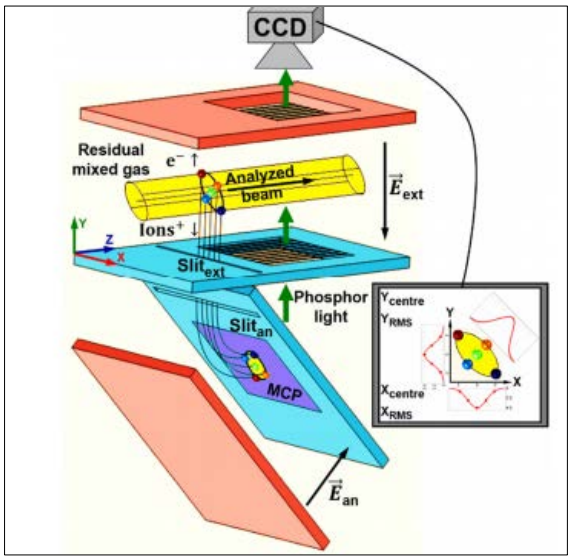

Fig. 7. Beam Cross-Section Monitor scheme [11].

Ionization profile monitors often suffer from artefacts in the measurement, the most important being the tails arising from the transverse drift of the electrons or ions during their travel towards the detector. More information on IPMs can be found in[2], [3].

Because of the low pressure of residual gas in some cases additional jet of O_2 can be used [13].

An interesting instrument is described in [14]. An ultrasonic 2-D jet of atomic Na (gas curtain) is produced in an oven followed by a collimation system. The Na-jet is inclined at 45° to the beam direction.

---

[1] S. Gavrilov, A. Feschenko, P. Reinhardt-Nickoulin and I. Vasilyev, Two-dimensional non-destructive diagnostics for accelerators by Beam Cross section Monitor, Journal of Instrumentation, V. 9, 2014, p. P01011.

[2] K. Satou, N. Hayashi, S. Lee, and T. Toyama, A prototype of residual gas ionization profile monitor for J–PARC RCS, 10th European Particle Accelerator Conference, EPAC2006, Edinburgh, UK, 2006, pp. 1163–1165.

[3] P. Forck, A. B. Bank, T. Giacomini, and A. Peters, Profile monitors based on residual gas interaction, 7th DIPAC, Lyons, France, 2005, pp. 223–227.

In [15] a special application of machine learning algorithms to the problem of reconstructing the actual beam profile from distorted measured profile is described.

Optical transition radiation screens

Optical Transition Radiation (OTR) monitors are widely used for profile measurements at linacs. The radiation is emitted when a charged particle beam crosses the boundary between the two media with different optical properties (here a thin reflecting screen, e.g. a silicon wafer covered with a thin layer of aluminum or silver in vacuum) [16].

When a fast electrically charged particle crosses the boundary between the two media of different dielectric constant, it emits radiation: "Optical Transition Radiation". The effect is known since 1946, but its usage for beam diagnostics has become more widely spread only over the last decade [17].

With respect to scintillator screens, usually about 1 mm thick, OTR has the advantage of being obtained from very thin foils, with much less scattering of the beam particles, and therefore less emittance increase. OTR is emitted from both sides of the foil. Fig. 8 shows the situation at the entrance side.

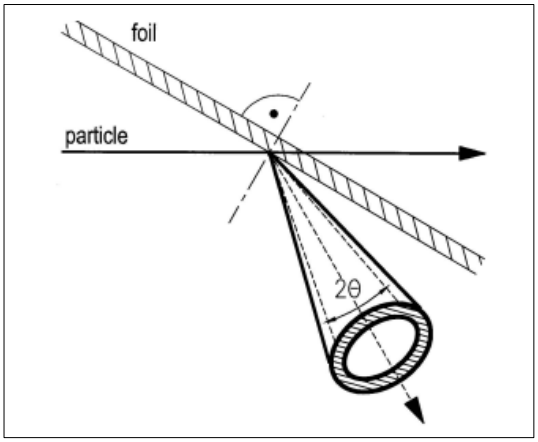

Fig. 8. OTR emitted from the entrance side of a foil. The radiation occurs into a hollow cone of opening-angle 2 θ around the «specular angle» (at which the particle would be reflected if it was a ray of light, and the foil a mirror), with θ = 1/γ of the particle [14].

Beam Scintillator Screens (fluorescence monitor)

A scintillator screen (often called phosphorescent, fluorescent or luminescent) is moved into the path of the beam [14].

Scintillators were the first particle detectors, more than a century ago. When accelerators, instead of cosmic radiation and radioactive samples, began to deliver particles, scintillators were the prime means to detect the existence of a beam and its location. In contrast to OTR, the scintillation light is emitted isotropically, i.e. there is no restriction on the observation geometry and both the screen and the camera can be placed under arbitrary angles with respect to each other [16].

The most common scintillator is used to be ZnS powder which, with some binder, was painted onto a metal plate. Such screens deliver green light and have high efficiency but are unfit to use in high vacuum and are burnt out at some 10^{14} protons/cm^2 at GeV energies. A great step forward was the formation of thick Al_20_3 layers on aluminum plates under simultaneous doping with Cr. Chemically, this is the same as ruby and the light emitted is red. These screens are fit for ultra-high vacuum and have a long lifetime (10^{20} to 10^{21} p/cm^2 at 50 MeV) [14].

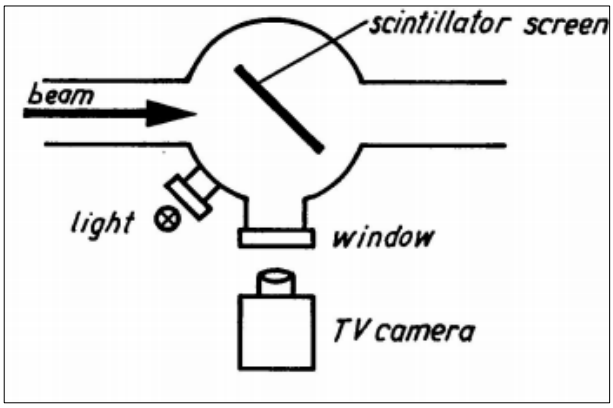

Fig. 9. Typical arrangement for observation of the beam position and size with a movable scintillator screen and a TV camera [14].

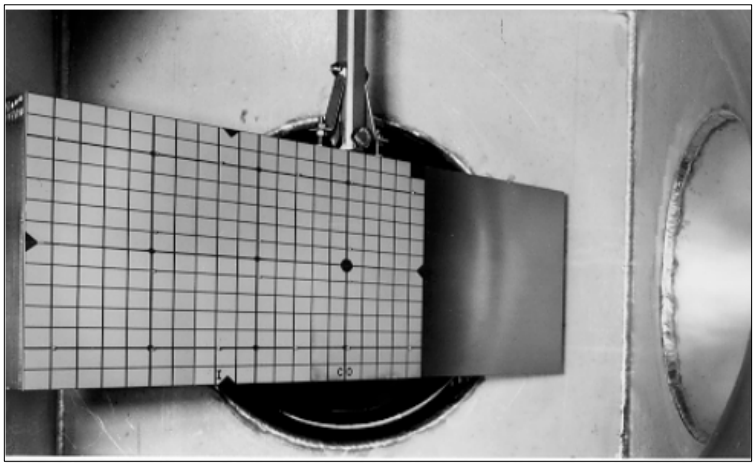

Fig. 10. Scintillator screen made from a Cr-doped Al_2O_3 plate with imprinted graticule [14].

The usage of few screen stations allows simultaneous determination of both the core region of the beam and its halo area [18]. The corresponding scheme is presented in Fig. 11.

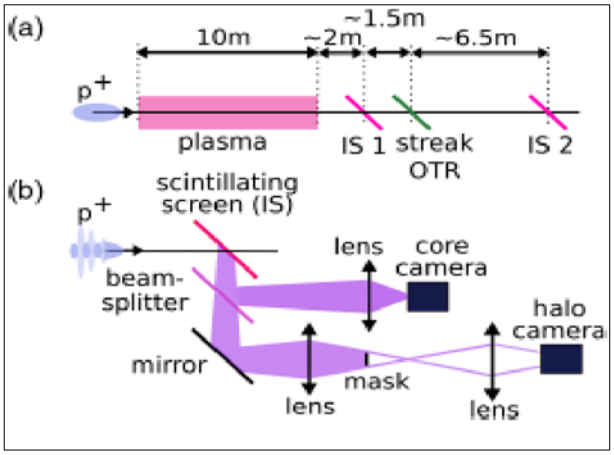

Fig. 11. (a) Schematic location of the imaging stations (IS1 and IS2) and of the OTR streak camera screen with respect to the plasma. The proton bunch moves from left to right. (b) Schematic drawing of the optical setup of the imaging station [18].

Synchrotron radiation monitor

Synchrotron radiation is emitted when an electron beam is accelerated by electromagnetic fields. This occurs especially efficiently in a particle accelerator and has been observed first in a synchrotron. Synchrotron radiation is a good source of information; it is also there for the taking (although the taking may be quite expensive) [19]. For diagnostic purposes, the light is extracted from the accelerator and transported to the measuring equipment by means of various optical elements, such as windows, mirrors, lenses and fibers. The receivers are TV cameras, CCDs, photo diodes (single or in an array), etc.

The information drawn may be simple, but very instructive, TV image of which enables to visually follow the evolution of the beam size; it may be a precise profile measurement; it may be a bunch length measurement with ps resolution which needs extremely fast oscilloscopes or a streak camera (that's where it gets expensive) [14].

An example of a synchrotron station is described in [20] (see Figs. 12, 13)

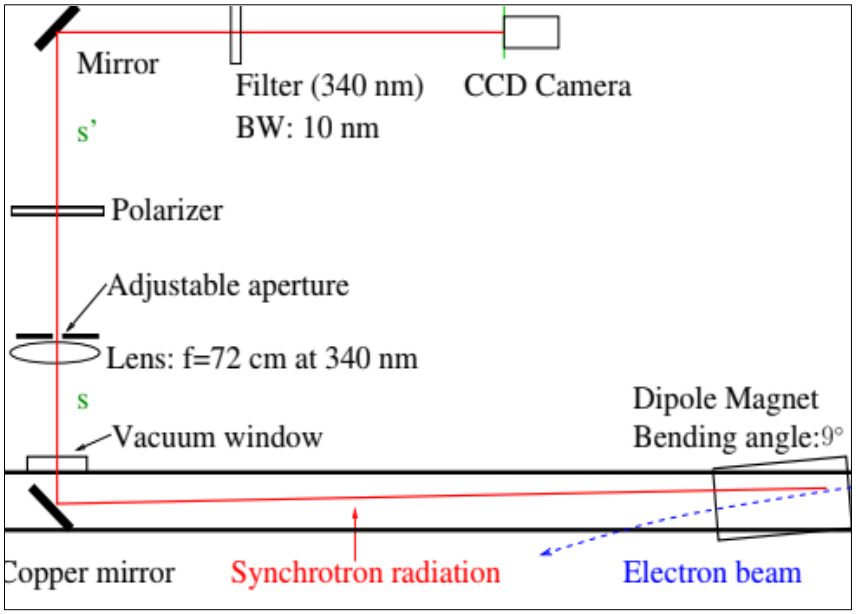

Fig. 12. The scheme of the transverse beam profile measurement system by synchrotron radiation. The direction of the synchrotron radiation is shown as a solid line (red), while the electron beam traverses a 9° dipole magnet along the dashed line (blue) [20].

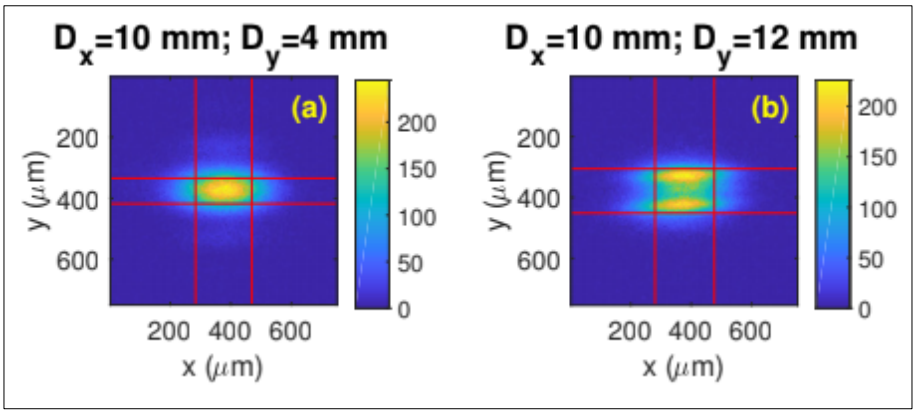

Fig. 13. Beam size measurements using the beam profile measurement system for a 0.1 mA single- bunch beam at 533 MeV. (a) and (b) are original images recorded by the CCD camera with horizontal aperture size D_x = 10 mm and the vertical aperture D_y = 4 mm or 12 mm, respectively [20].

Detailed description of an interferometer system and an imaging system using visible synchrotron radiation is presented in [21].

In [22] a technique for full reconstruction of the transverse beam profile based on a rotating double-pinhole mask is described.

Laser wire scanner

Another type of non-intercepting 1D pole monitor is the laser wire scanner. This device is based on the inverse Compton scattering (ICS) described before and is

thus only available for electron and positron beams. The basic concept is quite simple and is depicted in Fig. 14. A powerful, well focused laser (referred to as the laser wire) is scanned across the beam to be measured, as is done in a traditional wire scanner. The photons of the laser interact with the high-energy electrons and create high-energy X-rays or γ-rays, with an energy boost of the order of γ^2. A detector downstream detects the flux of those particles [2].

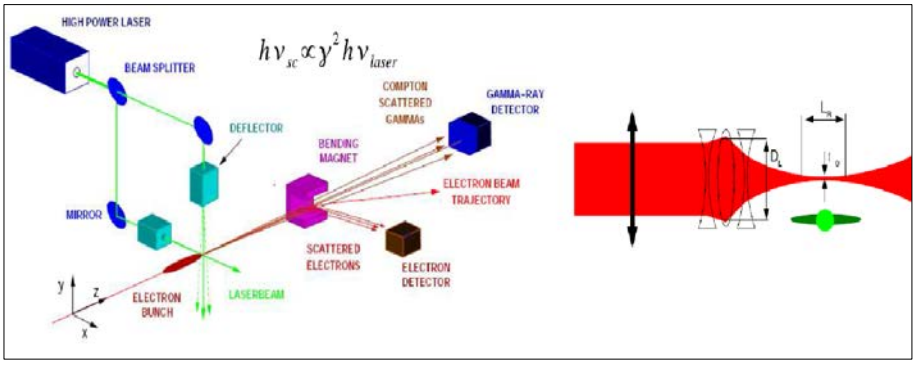

Fig. 14. The Scheme of a laser wire scanner system (left) and details of the laser focusing system (right) [2].

2. Vibrating wire monitors for beam profile measurement

The first instruments based on the vibrating wire technologies were developed in the late 1920s. Today the area of application of this technique expanded and different vibrating wire based sensors and monitors are used for measuring strain, displacement, piezometric level, pressure, angle and moment of rotation, viscosity of the media, and ultralow thermometry. The operating principle is based on the measurement of the change in the frequency of a vibrating wire depending on the physical parameters of the wire and environment in which oscillations take place. The advantages of properly constructed vibrating wire sensors are inherent long-term stability, high precision and resolution, good reproducibility and small hysteresis. The frequency signal of vibrating wire sensors is imperturbable and can be transmitted over long cable without degradation. It is also important to note a small zero drift and minimum change in sensitivity during a long time. An important parameter of vibrating wire-based sensors is their capability to operate in hard conditions [23, 24].

Original vibrating wire sensors and monitors for the beam instrumentation in accelerators were developed since 1999 [25]. The operating principle of sensors is based on the measurement of the change in the frequency of a vibrating wire depending on wire temperature. Instead of traditionally used steel wires excited into transverse vibration with the help of an electromagnet the interaction of AC current through the wire with a permanent magnet is used. This allows using non-steel wires and occurring very stable wire oscillations (less than 0.005 Hz in 5000 Hz full range). In accelerator diagnostics, vibrating wire monitors (VWM) are mainly aimed at measuring the transversal profile of different types of beams. The thermal principle of operation allows measuring charged particles, photons in a wide range of wavelengths and even neutrons [26, 27].

2.1 Physical Principles

The operating principle of vibrating wire sensors is based on the measurement of the change in frequency of a vibrating wire, which is stretched on a support, depending on the physical parameters of the wire and environment in which oscillations take place.

We take an electromechanical resonator with a metallic vibrating wire excited by the interaction of a current with a permanent magnetic field as a base for the VWM of

precise measurements of electron and proton beam profiles. The view of a typical VWM is presented in Fig. 15.

The interaction of the beam with the wire mainly causes the heating of the wire. The corresponding change of the wire's natural oscillations frequency provides information on its temperature and accordingly on the quantity of particles/photons of the beam penetrating the wire.

The thermal method of measurement also allows registering fluxes of neutrons and photons.

A vibrating wire based electromechanical resonator can be roughly represented as a support with a strained vibrating wire. The ends of the wire are rigidly fastened by special clips, so the length of the wire is really defined by the distance between these clips (we suppose that the base is much more rigid than the wire). As a background of development, we used an electromechanical resonator with a metallic wire vibrating which is excited by the interaction of a current with a permanent magnetic field.

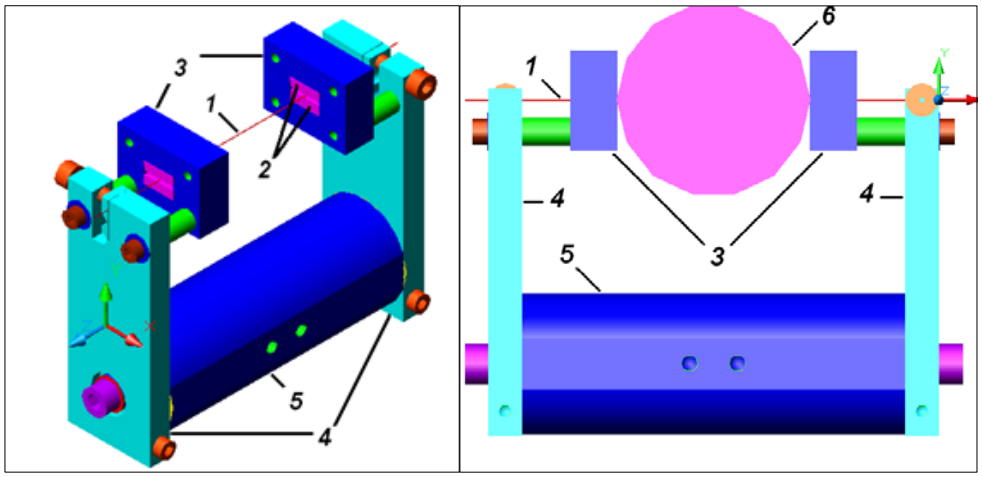

(a) (b)

Fig. 15. (a) Main view of the monitor with an aperture of 40 mm and a wire length of 80 mm: 1 – vibrating wire, 2 − magnets, 3 − magnet poles, 4 − clamps, 5 − basis. (b) The aperture of the monitor is defined by the circle 6 placed between the magnetic poles [1].

[1] M.A.Aginian, S.G.Arutunian, D.Choe, M.Chung, G.S.Harutyunyan, S.-Y.Kim, E.G.Lazareva, A. V. Margaryan, Precise out-vacuum proton beam monitoring system based on vibrating wire, Journal of Contemporary Physics (Armenian Academy of Sciences), 2017, Volume 52, Issue 2, pp 110–120.

The frequency of the second harmonics of the wire oscillations can be written in the form

$$F_0 = \frac{1}{L}\sqrt{\sigma_0 / \rho}\,. \tag{1}$$

Here σ is the tension of the wire with length L, ρ is the density of the wire material.

The parameters in (1) are undergoing temperature changes in the following way:

$$\frac{\Delta L}{L} = \alpha_B \Delta T\,, \tag{2}$$

where α_B is expansion coefficient of the base (here we use the above assumption that the length of the wire is defined by base characteristics),

$$\frac{\Delta \rho}{\rho} = -3\alpha_W \Delta T\,, \tag{3}$$

where α_W is expansion coefficient of the wire.

For change of the wire tension, we should use the Hook's law:

$$\Delta\sigma = E_W \frac{\Delta L}{L} = E_W \alpha_W \Delta T\,, \tag{4}$$

where E_W is wire material elasticity modulus and accordingly

$$\frac{\Delta\sigma}{\sigma} = \frac{E_W}{\sigma}\alpha_W \Delta T\,. \tag{5}$$

Values of expansion coefficients for metals are in the range of few units of 10^{-6} to $2*10^{-5}$ K^{-1}. Thus at temperature shifts of 1 K the relative changes of the length and density are about 1E-5. In case of tension change we have the additional factor E_W / σ, which is very large. E.g. for stainless steel (AISI 316) E_W =190-210 GPa and tensile strength 460-860 MPa. For wire initial tension we used 70% of tensile strength (assumed 700 MPa for used in VWM wire) so E_W / σ is about 400. From these simple estimations one can see that dependence on the temperature for ρ and L is negligible compared with the sigma temperature dependence.

For more detailed analysis, we introduce three temperatures:

$T_A(t)$ - ambient temperature

$T_B(t)$ - temperature of VWM base

$T_W(t)$ - temperature of VWM wire

At experiment start we have:

$$T_A(0) = T_B(0) = T_W(0) = T_0$$

(the T_0 is initial temperature) and

$$F(0) = \frac{1}{L}\sqrt{\sigma_o / \rho}\,. \tag{6}$$

At measuring time t:

$$F(0) = \frac{1}{L}\sqrt{(\sigma_o + E_B\alpha_B(T_B(t) - T_0) - E_W\alpha_W(T_W(t) - T_0)) / \rho} \tag{7}$$

The thermal inertia of the base is much larger than the thermal inertia of the wire.

As one can see, the frequency response accumulates the signal of the wire temperature change and is also subject to the base temperature changes (in the case of longtime experiment this will be perceived as a drift of the initial frequency).

First, we investigate what happens when all temperatures (basis and wire) follow a slowly changed ambient temperature $(T_B(t) = T_W(t) = T_A(t))$.

$$F_A(t) = \frac{1}{L}\sqrt{(\sigma_o + (E_B\alpha_B - E_W\alpha_W)(T_A(t) - T_0)) / \rho} \tag{8}$$

One can see that in a special case

$$E_B\alpha_B - E_W\alpha_W = 0, \tag{9}$$

the frequency does not depend on the ambient temperature. We call this type of sensor a temperature compensated VWM.

For the temperature compensated VWM one can divide the temperature into two terms: wire temperature depending only on agent influence and ambient variations

$$T_W(t) = T_A(t) + T_W^{ag}(t) - T_0\,. \tag{10}$$

Finally, for this temperature compensated VWM we have

$$F(t) = \frac{1}{L}\sqrt{(\sigma_o - E_W \alpha_W)(T_W^{ag}(t) - T_0))/\rho}\cdot \qquad (11)$$

Practically the condition of VWM thermal compensation (Eqs. 9, 11) is hard to realize due to the fact that the wire and the base are manufactured from different materials. But even if the base and the wire are from the same material (e.g. from stainless steel) there is some difference in these material parameters, so Eq. 11 isn`t satisfied precisely. Besides, one should take into account completely the different thermal inertia of a thin wire and massive base.

A good choice is to manufacture a sensor with two vibrating wires, one is exposed onto the beam and the second one is used as reference for taking into account slow changes of ambient temperature (see Fig. 16).

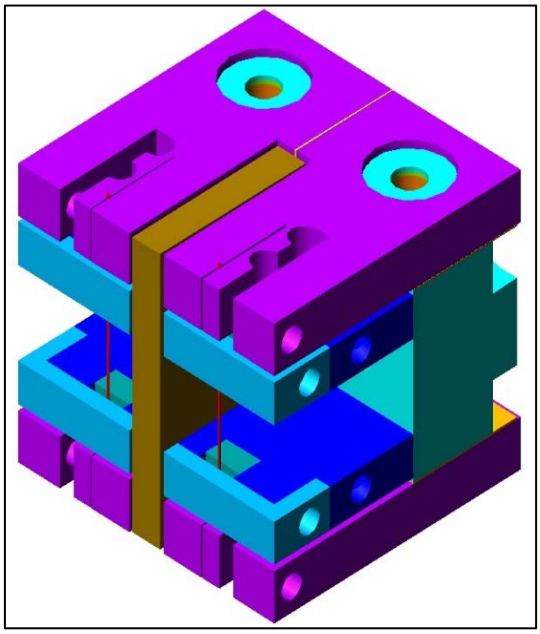

Fig.16. Double wire vibrating wire monitor (DW-VWM).

In this case the VWM consists of two identical strings on a common base. One wire (first, temperature $T'_W(t)$) is exposed to the beam; the other (second, temperature $T''_W(t)$) is served as a reference. For the second wire, we assume $T''_W(t) = T_B(t)$.

As a result, to determine the temperature of the wire, we have two equations

$$F'(t) = \frac{1}{L}\sqrt{(\sigma'_0 + E_B\alpha_B(T_B(t) - T_0) - E_W\alpha_W)(T'_W(t) - T_0))/\rho} \qquad (12)$$

$$F''(t) = \frac{1}{L}\sqrt{(\sigma_0'' + (T_B(t) - T_0)(E_B\alpha_B - E_W\alpha_W))/\rho} \quad (13)$$

From the second equation we obtain:

$$T_B(t) - T_0 = ((F''(t))^2 - (F_0'')^2)L^2\rho/(E_B\alpha_B - E_W\alpha_W), \quad (14)$$

where

$$F_0'' = F''(0) = \frac{1}{L}\sqrt{\sigma_0''/\rho} \quad (15)$$

and for the change of wire temperature:

$$F'(t) = \frac{1}{L}\sqrt{(\sigma_0' + E_B\alpha_B(T_B(t) - T_0) - E_W\alpha_W(T_W'(t) - T_0))/\rho}. \quad (16)$$

From this formula one can obtain finally:

$$T_W'(t) - T_0 = L^2\rho\left[\frac{E_B\alpha_B}{E_W\alpha_W(E_B\alpha_B - E_W\alpha_W)}\left[(F''(t))^2 - (F_0''(t))^2\right] - \frac{1}{E_W\alpha_W}\left[(F'(t))^2 - (F_0')^2\right]\right]$$
. (17)

2.2. Thermal balance of VWM

The beam penetrating the wire loses some energy and heats the wire. The wire temperature increase relative to the initial temperature can be calculated by the equation of balance between the power deposited into the wire and heat sink through all possible thermal mechanisms: conduction along the wire to the end clips, convection losses to ambient atmosphere (in case if air or other atmosphere is present), and losses through the radiation to ambient space. It is assumed that there are no other heat sources except for the beam impact, and that the profile of the balanced temperature has a triangle profile (this is a sufficiently close approximation). The balance equation is written as:

$$W_{\text{beam}} = W_\lambda + W_{\text{rad}} + W_{\text{conv}}, \quad (18)$$

where W_{beam} is the deposited power from the beam into the wire and

$$W_\lambda = 8(T - T_0)\lambda S/L \quad (19)$$

is the conductive heat sink,

$$W_{\text{rad}} = \varepsilon\sigma_{\text{ST\_B}} T_{\text{W}}^4 \pi dL - \varepsilon\sigma_{\text{ST\_B}} T_0^4 \pi dL \tag{20}$$

is the heat sink through the radiation (here we consider temperatures in Kelvin),

$$W_{\text{conv}} = \delta(T_{\text{W}} - T_0)\alpha_{\text{conv}} \pi dL \tag{21}$$

is the convection heat sink.

Here T_0 is the ambient temperature, $T_{\text{W}} = ((T + T_0)/2)$ is the wire mean temperature d, L are the diameter and length of the wire, S is the wire cross section, λ is the thermal conductivity of the wire material, $\sigma_{\text{ST\_B}}$ is the Stefan-Boltzmann constant, ε the radiation coefficient of the wire, α_{conv} the convection heat transfer coefficient, $\delta = 1$ if the wire placed in atmosphere, and $\delta = 0$ if the wire is placed in vacuum.

Introducing the parameter $\Delta T = (T_{\text{W,MEAN}} - T_0)/2)$ (mean overheating of the wire), the following relation between ΔT and W_{beam} can be found:

$$\Delta T = \frac{W_{beam}}{8\lambda S / L + 4\varepsilon\sigma_{ST\text{-}B} T_0^3 \pi dL + \delta\alpha_{conv} \pi dL}. \tag{22}$$

For parameter α_{conv} we use the equation for convection of the cylinder by air with the speed of ν

$$\alpha_{\text{CONV}} = 4.13 \frac{\nu^{0.8}}{d^{0.2}}. \tag{23}$$

An important parameter of the VWM is its response time which, in case of air, can be estimated as follows (more details see in section 2.7):

$$\tau = \frac{c\rho}{8(\lambda / L^2 + 2\varepsilon\sigma_{ST\text{-}B} T_0^3 / d + \alpha_{conv} / 2d)} \tag{24}$$

2.3. VWM typical samples

Below we present a few estimations for a VWM with a wire from different materials: tungsten and stainless steel.

The frequency of the wire for a stable autogeneration process should exceed 1000 Hz (experimentally checked information based on our experience), so the tension of the wire will be greater than the specific limit for given VWM parameters (value is calculated by formula (1)). The tension of the wire should be in the range of linear dependence of the wire material. We used 0.7 of tensile force, for stainless steel, which is about 700 MPa. Caused by the wire heating, the frequency decreases from the initial value to the 1000 Hz lower limit. Therefore, for enlargement of the VWM range it is preferable to choose the initial tension near the upper limit. The graphics of dependence of VWM frequency on wire tension for tungsten and stainless steel are presented in Fig. 17.

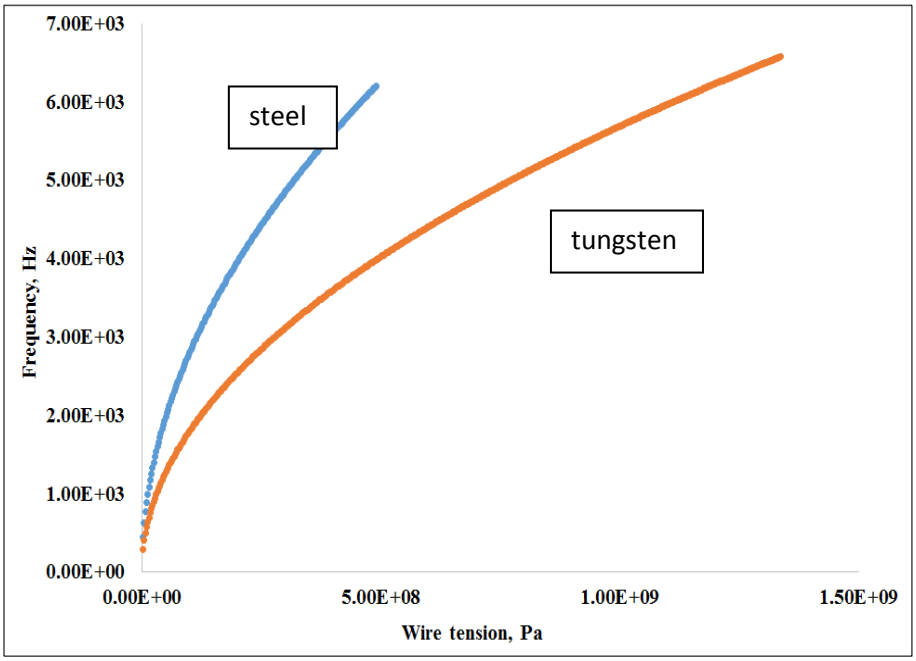

Fig. 17. Frequency on tension (Pa) for tungsten (orange) and stainless steel (blue).

In Fig. 18 we present the dependence of VWM frequency on wire temperature for tungsten and stainless steel. One can see that the temperature range of tungsten wire is much larger than the range of stainless steel. But on the other hand, the sensitivity of stainless steel is higher than that of tungsten wire.

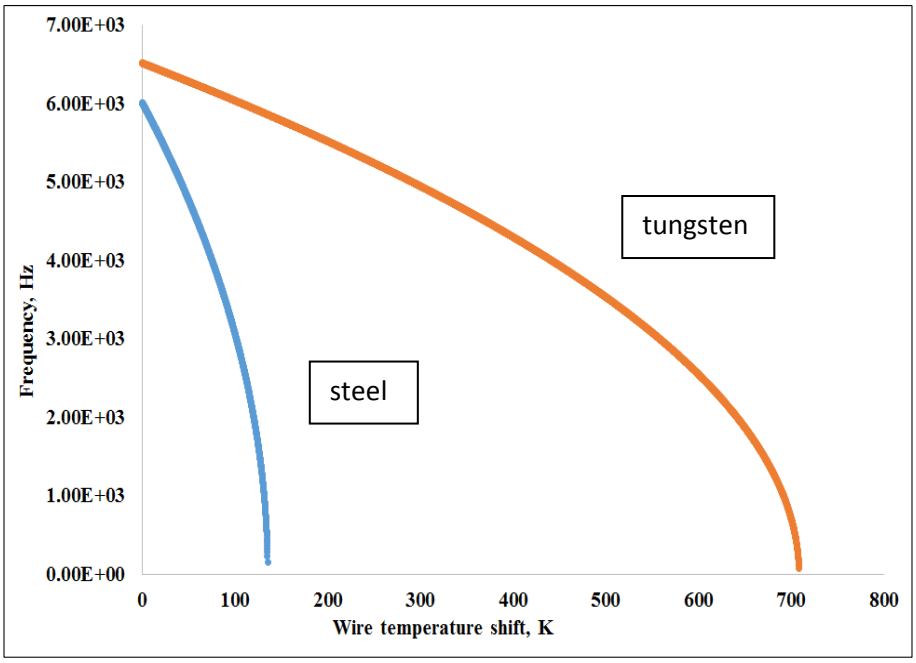

Fig. 18. Frequency on wire temperature shift for tungsten (orange) and stainless steel (blue).

In Tab. 1 we accumulate thermal parameters of a VWM with tungsten wire. The VWM is supposed to operate in air or in vacuum. In the last case, the convection losses are absent. All power values are given in Watt units.

Table 1. Thermal parameters of VWM with tungsten wire

Wire temperature rise, K	Frequency, Hz	W_{conv}, W	W_{λ}, W	W_{rad}, W	$W_{total\ in\ air}$, W	$W_{total\ in\ vacuum}$, W
0	6.51E+03	0.00E+00	0.00E+00	0.00E+00	0.00E+00	0.00E+00
0.001	6.51E+03	2.14E-07	2.72E-07	5.02E-08	5.36E-07	3.22E-07
0.01	6.51E+03	2.14E-06	2.72E-06	5.02E-07	5.36E-06	3.22E-06
0.1	6.51E+03	2.14E-05	2.72E-05	5.02E-06	5.36E-05	3.22E-05
1	6.51E+03	2.14E-04	2.72E-04	5.04E-05	5.36E-04	3.22E-04
10	6.47E+03	2.14E-03	2.72E-03	5.28E-04	5.38E-03	3.25E-03
100	6.04E+03	2.14E-02	2.72E-02	8.22E-03	5.68E-02	3.54E-02
200	5.52E+03	4.27E-02	5.43E-02	2.58E-02	1.23E-01	8.01E-02
400	4.30E+03	8.55E-02	1.09E-01	1.11E-01	3.06E-01	2.20E-01
600	2.55E+03	1.28E-01	1.63E-01	3.14E-01	6.05E-01	4.77E-01

On can see that only at low overheating (less than 10 ^{0}C) in air the convection losses dominate:

$$W_{CONV} >> W_{\lambda} >> W_{RAD} \qquad (25)$$

In Tab. 2 we accumulate the same thermal parameters of VWM with stainless steel wire.

Table 2. Thermal parameters of VWM with stainless steel wire

Wire temperature rise, K	Frequency, Hz	W_{conv}, W	W_{λ}, W	W_{rad}, W	$W_{total\ in\ air}$, W	$W_{total\ in\ vac}$, W
0	6.01E+03	0.00E+00	0.00E+00	0.00E+00	0.00E+00	0.00E+00
0.001	6.01E+03	2.14E-07	2.67E-08	5.02E-08	2.91E-07	7.69E-08
0.01	6.01E+03	2.14E-06	2.67E-07	5.02E-07	2.91E-06	7.69E-07
0.1	6.01E+03	2.14E-05	2.67E-06	5.02E-06	2.91E-05	7.69E-06
1	5.99E+03	2.14E-04	2.67E-05	5.04E-05	2.91E-04	7.71E-05
10	5.78E+03	2.14E-03	2.67E-04	5.28E-04	2.93E-03	7.95E-04
100	3.07E+03	2.14E-02	2.67E-03	8.22E-03	3.23E-02	1.09E-02

2.4. Wire heating by DC current

To demonstrate VWM operation, it is possible to model the flux of measuring particles by a DC current through the wire. For this purpose, in the autogeneration scheme of the VWM we introduced a special capacitor that allows separating this DC current from the AC current of autogeneration. In this case, an external DC current is served as a source of heat. The corresponding dissipated power is calculated by the formula

$$W_{DC} = I^2 R_W = \rho_{el} L / S, \quad (26)$$

where R_W is the resistance of the wire (ρ_{el} is electrical resistivity of the wire, S is wire cross section).

The values of power dissipated into the wire from tungsten and stainless steel are presented in Tab. 3.

Table 3. DC current heat sources for tungsten I_{W} and stainless steel I_{SS}.

I_{W}, A	W_{DC}, W	I_{SS}, A	W_{DC}, SS 316
0	0.00E+00	0.00E+00	0.00E+00
1.00E-03	2.75E-07	1.00E-03	3.77E-06
1.00E-02	2.75E-05	5.00E-03	9.42E-05
1.00E-01	2.75E-03	1.00E-02	3.77E-04
2.00E-01	1.10E-02	2.00E-02	1.51E-03
4.00E-01	4.40E-02	3.00E-02	3.39E-03
6.00E-01	9.90E-02	4.00E-02	6.03E-03
8.00E-01	1.76E-01	5.00E-02	9.42E-03
1.00E+00	2.75E-01	6.00E-02	1.36E-02
1.20E+00	3.96E-01	7.00E-02	1.85E-02
1.40E+00	5.39E-01	8.00E-02	2.41E-02
		9.00E-02	3.05E-02

2.5. Frequency measurement algorithm

The measurement of the wire oscillation frequency F in the time gate g is done by counting of N_{q} periods using a precise quartz generator (generating a high frequency F_{q}) in N_{f} numbers of the full wire frequency periods that approximately cover the time gate, (see Fig. 19). The wire oscillation periods are fixed precisely using a zero-crossing mechanism. From the equality

$$\frac{N_{\mathrm{f}}}{F} = \frac{N_{\mathrm{q}}}{F_{\mathrm{q}}} \approx g \tag{27}$$

an equation for the value of the frequency of the vibrating wire is found:

$$F = F_{\mathrm{q}} \frac{N_{\mathrm{f}}}{N_{\mathrm{q}}}. \tag{28}$$

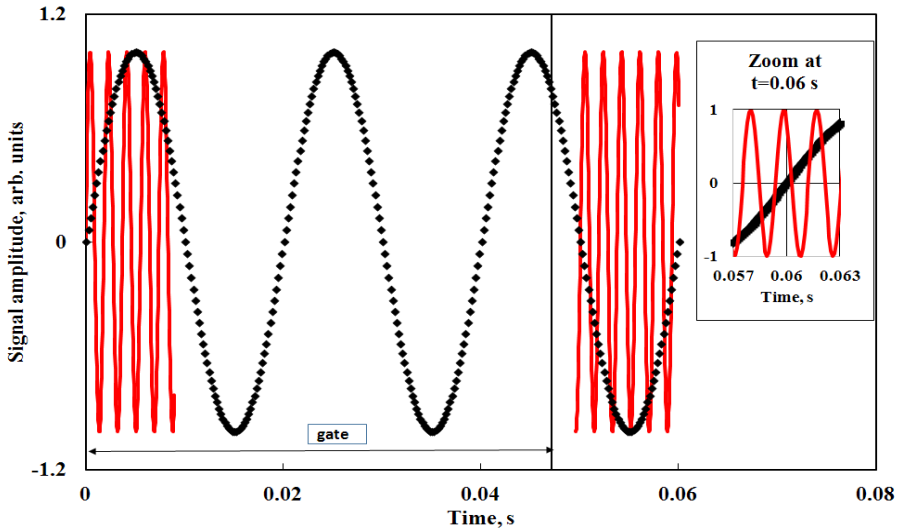

Fig. 19. The principle of wire oscillation frequency measurement: solid line – quartz high frequency, diamonds are frequency signal of the wire, vertical line – preliminary gate set g. In the insert the zoom around t = 0.06 s is presented (see more detailed in[1]).

At the end of the time frame the crossing of high frequency can happen at any phase of the quartz generator period (see insert in Fig. 19), so the number of quartz periods can vary on one digit. The corresponding accuracy of the method is presented by the following equation

$$\frac{\Delta F}{F} \approx \frac{1}{N_q} \approx \frac{1}{gF_q}. \qquad (29)$$

Therefore, the relative accuracy of measurements at 1 s sampling and 1 MHz quartz is ~ 10^{-6}.

2.6. Beam losses in matter

The main parameter for the given configuration of measured particles and VWM with the wire of specific material is the quantity of energy that one particle loses when penetrating the wire (parameter W_{beam} in formula (18)). The rule of calculations is strongly dependent on the type of particles.

Protons/ions

[1] S.G.Arutunian, G.S.Harutynyan, D.Choe, M.Chung, E.G.Lazareva, A.V.Margaryan, Effects of scanning speed on the laser beam profile measurements by vibrating wire, Journal of Contemporary Physics (Armenian Academy of Sciences), 2017, Vol. 52, 4, pp 366–374.

For heavy particles (protons and ions) the parameter W_{beam} in formula (18) is determined by ionization losses of particles penetrating the wire material. Equation for specific ionization losses dE/dx of a particle with mass $M >> m_{\text{e}}$ (m_{e} - electron mass) and velocity v is known as the Bethe−Bloch formula, which is the basic expression used for energy loss calculations [28],

$$-\frac{dE}{dx}=2\pi N_{\text{A}} r_{\text{e}}^2 m_{\text{e}} c^2 \rho \frac{Z}{A}\frac{z^2}{\beta^2}\left[\ln\left(\frac{2m_e c^2\gamma^2\beta^2 W_{\max}}{\Phi^2}\right)-2\beta^2-\delta-2\frac{C}{z}\right] \qquad (30)$$

where $2\pi N_{\text{A}} r_{\text{e}}^2 m_{\text{e}} c^2$ =0.1535×10^{-4} MeV·m^2/mol, N_{A} =6.022×1023 mol^{-1} − Avogadro's number, r_e =2.817×10^{-15} m is the classical electron radius, ρ is the density of absorbing material in g/cm^3, Z is the atomic number of the absorbing material, z the charge of the incident particle in units of electron charge, A is the atomic weight of the absorbing material in g/mol, Φ the mean ionization potential in eV, $\beta = v/c$; $\gamma=1/\sqrt{1-\beta^2}$, c is the speed of light, δ is the amendment, which takes into account the effect of medium density, C the correction effect of the electrons' binding on K- and L- shells, and $W_{\max}$ the maximum energy transfer in a single collision. The maximum energy transfer in the case of proton mass $m_{\text{p}} >> m_{\text{e}}$ is $W_{\max} \approx 2m_e c^2\gamma^2\beta^2$. For electrons and positrons, the Bethe−Bloch formula differs from Eq. (30).

In Tab. 4 some typical values for the proton ionization losses in tungsten (Z =74, A =183.84 g/mol, ρ = 19.3 g/cm^3) are presented without corrections in two proton energy ranges.

Table 4. Ionization losses dE_{p}/dx for proton in the tungsten (E_{p} is the proton kinetic energy).

E_{p}, MeV	dE_{p}/dx, MeV/cm	E_{p}, MeV	dE_{p}/dx, MeV/cm
10	384.63	1000	23.87
11	359.92	2000	22.63
12	338.57	3000	23.04
13	319.92	4000	23.66
14	303.46	5000	24.29
15	288.83	6000	24.88

16	275.73	7000	25.43
17	263.91	8000	25.92
18	253.20	9000	26.37
19	243.44	10000	26.79
20	234.50		
21	226.29		
22	218.71		
23	211.70		
24	205.18		
25	199.11		

For one proton, the energy loss δ_{p} in the wire can be roughly approximated as

$$\delta_p = \left(\frac{dE_p}{dx} \right) \times (\pi d / 4) \cdot \tag{31}$$

Some of the proton energy losses will be transferred to the heat in the wire material. The ratio of this energy transport $\varepsilon_{\mathrm{heat}}$≈0.3 depends on proton energy, parameters of the wire material and the wire geometry. We set $\varepsilon_{\mathrm{heat}}$≈0.3.

The equation that determines the frequency shift of the wire oscillation depends on the proton beam current I_{p} penetrating the wire:

$$\frac{\Delta F}{F_0} = -\frac{E}{2\sigma_0} \frac{\alpha \varepsilon_{heat} (\delta_p I_p / e)}{\left[8\lambda S / L + 4\varepsilon \sigma_{ST\text{-}B} T_0^3 \pi dL + \eta \alpha_{conv} \pi dL \right]} \tag{32}$$

where $F_0 = (1/L)\sqrt{\sigma_0 / \rho}$ is the initial frequency of the wire vibrating on the second harmonics σ_0 is the initial tension of the wire, ρ is the density of wire material, α is the wire material's coefficient of thermal expansion, and E is the elasticity module of the wire material.

Electrons and positrons

To estimate the electron losses in matter one should consider more processes besides the ionization [2]:

creation of electron-positron pairs,

secondary electron emission (SEM, low energy),

emission of photons,

elastic and inelastic scattering,

dislocations,

production of secondary particles (high energy),

Cherenkov radiation,

bremsstrahlung,

optical transition radiation (OTR).

Corresponding processes for electrons moving in lead are presented in Fig. 20.

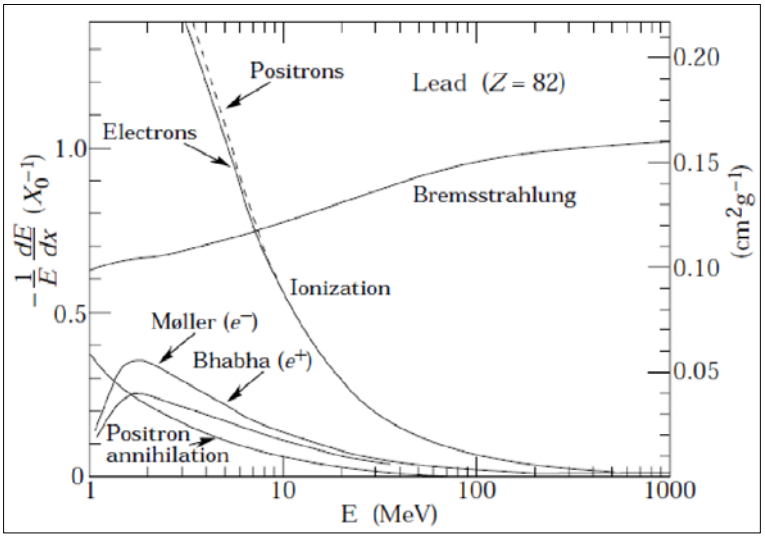

Fig. 20. Fractional energy loss per radiation length in lead as a function of electron or positron energy. Electron (positron) scattering is considered as ionization when the energy loss per collision is below 0.255 MeV, and as Moller (Bhabha) scattering when it is above [29].

Modified Bethe-Bloch formulae for ionization losses for electrons and positrons can be found in Ref [30].

Muons

An interesting type of accelerators are muon accelerators that offer unique potential for particle physics applications. The concept of the muon collider was first proposed in 1969 [31]. The special Muon Accelerator Program (MAP) was created in 2010 aimed at developing the concepts and technologies required for Muon Colliders and Neutrino Factories [32]. For these type of machines we present in Fig. 21 the muon losses in copper.

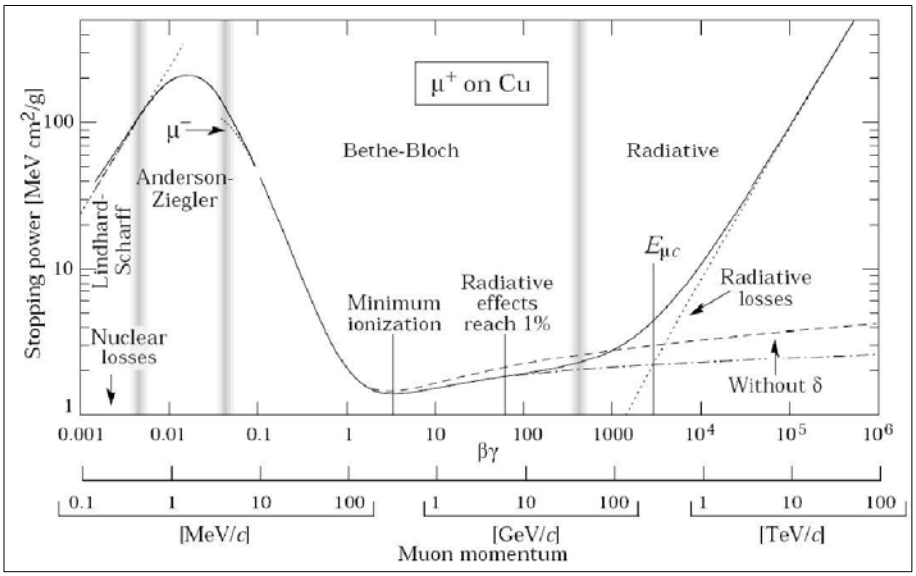

Fig. 21. The dE/dx curve for positive muons in copper, the same curve describes well other elementary particles with q=1 and different materials. Note, that the horizontal axis is given in terms of particle momentum and not particle energy. For reference, $\beta\gamma$ = 1 corresponds to a E_k of 212 keV for electrons and 390 MeV for protons [2] (βc and $mc^2\gamma$ are the velocity and energy of the particle).

2.7. VWM parameters choice

In case of application of the VWM in a specific accelerator we have developed a special program ***VWM Parameters Choice*** for choosing proper parameters of VWM including its geometrical characteristics depending on the measured type of beam particles and its energy, the approximate beam sizes and operation conditions. Below we describe in more detail how to use this program.

1. Enter the initial parameters

Before proceeding with the program after its run we need to enter the initial parameters in the working window of the program (see Fig. 22):

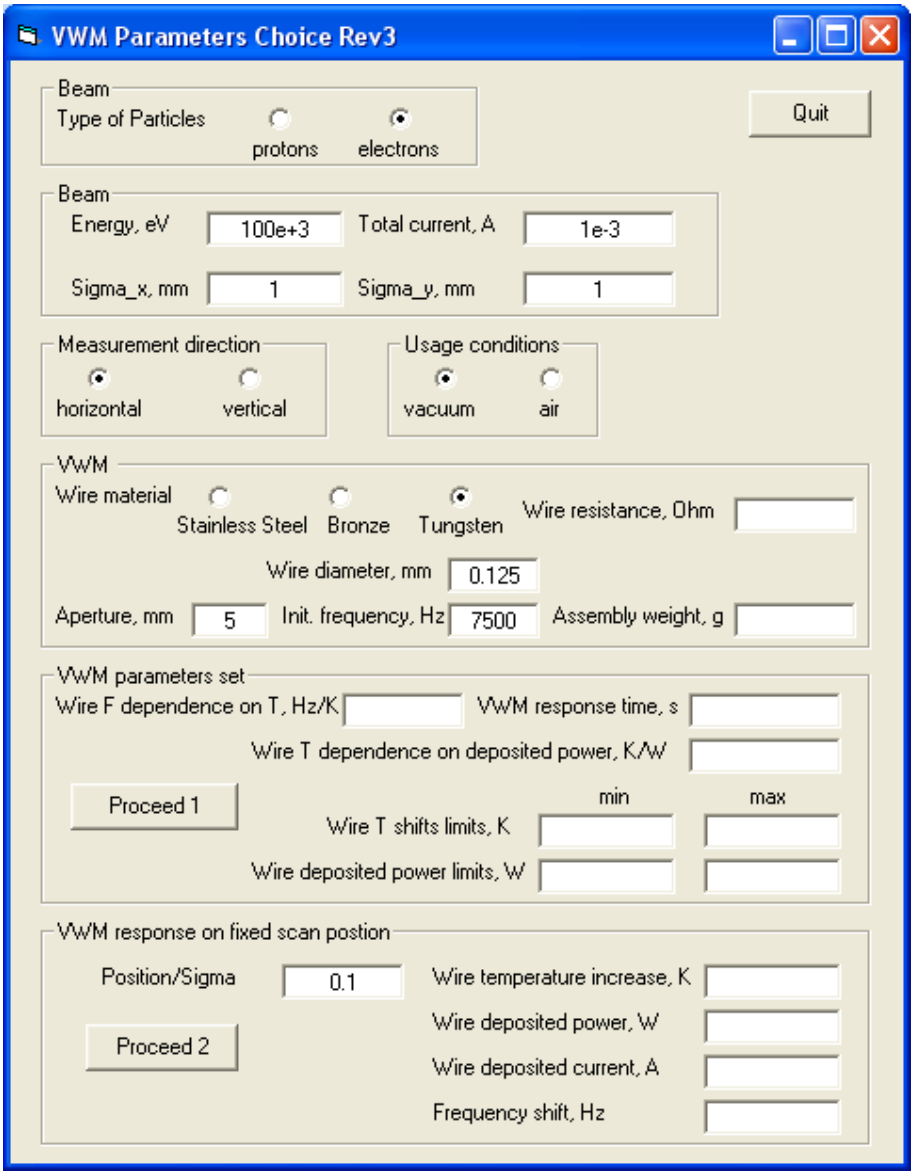

Fig. 22. Main view of the program ***VWM Parameters Choice.***

The set of these parameters and labels on the window are marked below with green color.

Initial frequency F_0 of the vibrating wire (second harmonic of natural oscillation) is defined by Eq. (1):

The corresponding weight needed for VWM wire assembling and resistance of the wire will appear at **Proceed 1** button.

2. Proceed 1 VWM parameters

Wire frequency **F dependence on** wire temperature **T** is defined by Eqs. (1-5):

$$\Delta F / \Delta T = \frac{E \alpha F_0}{2\sigma_0}.,$$ (33)

where α is the wire material coefficient of thermal expansion, E is the wire material modulus of elasticity.

VWM response time is defined by three thermal processes: heat sink through the wire material, radiation losses and convection losses (in case of air).

Response time via thermal conductivity mechanism:

$$\tau_\lambda = \frac{c\rho}{8(\lambda / L^2)},$$ (34)

where c is specific heat, λ is thermal conductivity coefficient.

Response time via radiation mechanism

$$\tau_{RAD} = \frac{c\rho}{8(2\varepsilon\sigma_{ST\_B} T_0^3 / d)},$$ (35)

where σ_{ST_B} is the Stefan–Boltzmann constant, T_0 is the wire initial temperature (room temperature is supposed), d is the wire diameter, ε is the emissivity of the wire surface (a measure of the ability of the wire surface to radiate energy).

Response time via convection mechanism in the air

$$\tau_{CONV} = \frac{c\rho}{8(\alpha_{CONV} / 2 / d)},$$ (36)

where α_{CONV} is coefficient of convective losses.

Response time of the wire:

$$\tau_{RESP} = \frac{1}{1/\tau_\lambda + 1/\tau_{RAD} + \delta / \tau_{CONV}},$$ (37)

where $\delta = 1$ in case of **air** and $\delta = 0$ in case of **vacuum**.

Wire temperature **T dependence on deposited power** is defined by Eq. (22).

The wire temperature **T shifts limits** are defined by the characteristics of the VWM electromechanical resonator and are for frequencies

$\Delta F_{MIN} = 0.01Hz$ (VWM resolution), (38)

$\Delta F_{MAX} = 2000Hz$ in case if initial frequency $F_0 > 3000Hz$ and (39)

$\Delta F_{MAX} = F_0 - 1000Hz$ in case if initial frequency $F_0 < 3000Hz$. (40)

By these values the wire temperature shifts are calculated.

Deposited power limits of VWM are calculated by the same values taking into account Eqs. (33) and (22). In the case presented on the picture below, the deposited power limits are

$W_{beam\_\min}$=6.8E-7 W and $W_{beam\_\max}$=1.3E-1 W with a dynamic range of the VWM of 5E+5.

3. Proceed 2: The dependence of VWM frequency shifts on the VWM position relative to the beam center.

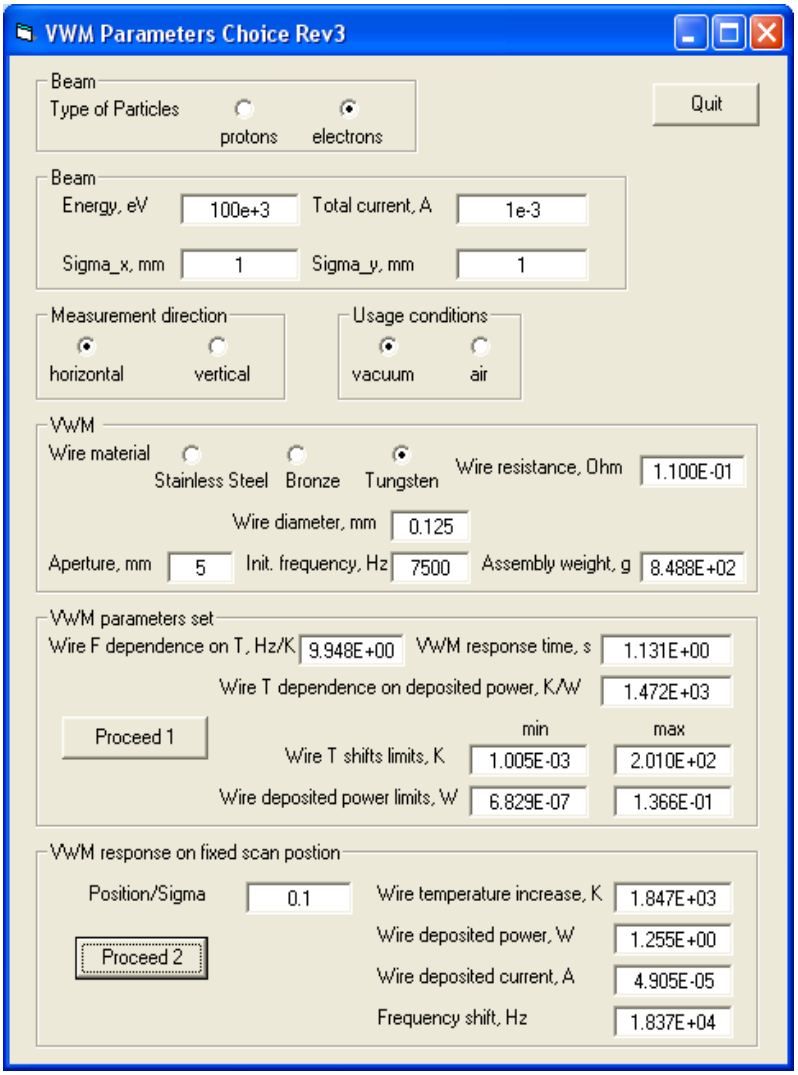

Fig. 23. Main view of the program prepared to **Proceed 2**.

Position/Sigma presents the position of the wire in units of beam sigma along the scan direction σ_{SCAN}, which is equal to σ_X (horizontal) or σ_Y (vertical) depending on the choice of measurement direction:

$\sigma_{SCAN} = \sigma_X$ and $\sigma_{TRAN} = \sigma_Y$ (case measurement direction **horizontal**), (41)

$\sigma_{SCAN} = \sigma_Y$ and $\sigma_{TRAN} = \sigma_X$ (case measurement direction **vertical**), (42)

where σ_{TRAN} describes the beam distribution along the wire direction (see Fig. 23).

The current of particles penetrating the wire I_W is described by:

$$I_W = I_0 * K_A * \frac{d}{\sqrt{2\pi}\sigma_{SCAN}} * \exp(-x^2 / 2) \qquad (43)$$

where I_0 is the beam **Total current**, x is the wire position in units of σ_{SCAN},

$K_A = \int_{-A/2}^{+A/2} dz * \frac{1}{\sqrt{2\pi}\sigma_{TRAN}} * \exp(-z^2 / 2 / \sigma_{TRAN}^2)$ describes the limitation of intersected wire particles cause by the limited **Aperture** A of the VWM.

Heat transfer from intersected wire particles depends on particles types and energy, wire material and geometry. To first order, in the present calculations we assume that heat transfer is described by ionization losses in the material including a heat transfer coefficient k defining what part of losses is really converted into the heat:

$$W_{beam} = k * I_W * E_Z, \qquad (44)$$

where $E_Z = \rho * E_{NORM}$.

The parameter E_{NORM} is calculated from the Bethe-Bloch formula and for 3 GeV protons it is about 1.5 MeV/cm^2/g. Indeed, this value depends only weakly on particle **Energy** and on the particle type in case of $E \geq 1GeV$. For electrons and muons one should calculate the beam losses according to section 2.6.

In the present case, the position $0.1*\sigma$ leads to a wire temperature increase above the maximum possible limit of about 200 K.

2.8. VWM application

Vibrating wire monitors are applicable in various configurations:

1. Single-wire monitors/scanners of average geometric dimensions with generation of the second harmonic of oscillations: the magnetic poles of the sensor for exciting the second harmonic are located along the edges of the wire, freeing the aperture for the beam, which is about half of the wire length. A typical application of such monitors is scanning the beam profile.

2. Double-wire beam position monitors: monitors with two wires spaced a few mm apart allow a differential method to control the beam shift between the wires. The

method of differentiation of signals of two wires can also be used to normalize monitors taking into account the influence of ambient temperature and the presence of other background besides the direct impact of the measured beam (one of the wire is exposed by the beam, the second wire is protected from the beam by a special screen and serves as a reference signal). In [1] a type of double-wire monitor with an aperture increased by 8 mm is presented. This modification has a shorter response time and can be used both in vacuum and in air.

A novel double-wire monitor of vibrating wire (DW-VWM) consists of two wires spaced by a screen. The monitor is being developed for the joint European-Japanese project IFMIF, specifically for the LIPAc accelerator (Linear IFMIF Prototype Accelerator) (for details see [2]). The specific feature here is the high accelerator current (about 125 mA of the average beam current), which dictates the need for precise measurement of the flux of lost particles and the halo region of the beam.

3. Multi-wires monitors: the use of several wires enables the simultaneous measurement of the beam profile without a scanning procedure, which can significantly reduce the measurement time. A five-wire monitor of this type was, for example, used to measure the profile of a synchrotron radiation beam at the APS ANL accelerator (measurements were made in the air)[3]. Since the synchrotron radiation is concentrated in the plane of the beam orbit, only the vertical beam profile was measured (the change in beam density depends on the vertical coordinate).

4. Large aperture monitors: such sensors are of interest for profiling large proton beams (up to 80 mm). Two types of such monitors are developed:

---

[1] Arutunian S.G., Decker G., Mailian M.R., Rosenbaum G. Transition thermal processes in vibrating wire monitor, DIPAC 2007, pp. 292-294.

[2] Overview of the IFMIF/EVEDA project, URL:
https://iopscience.iop.org/article/10.1088/1741-4326/aa6a6a/pdf

[3] G.Decker, R. Dejus, S.Arutunian, M.Mailian, I.Vasiniuk. Hard X-ray synchrotron radiation measurements at the APS with vibrating wire monitor. In Beam Instrumentation Workshop, BIW08; 2008; Lake Tahoe, USA. p. 36-40.

- direct action of the beam on a vibrating wire: a special scheme of shock excitation of the process of autogeneration of oscillations is added to the electronic circuit,
- yoke type with two mechanically connected wires: a non-vibrating target wire of increased length and a vibrating wire measuring the change in the tension of the target wire exposed by the beam. Measurement of the temperature/tension of the target wire was carried out with the help of a special link between the two wires. The aperture of such monitors can reach 80 mm.

5. VWM with multilayer (composite) wire. A special type of VWM with wire covered by gadolinium layer was developed for thermal neutron beam profiling [33]. Two unique properties are combined here – the unprecedented sensitivity of the natural frequency of a clamped vibrating wire to the wire temperature, and a remarkable ability of some gadolinium isotopes to neutron capture. 157Gd has the highest thermal neutron capture cross section of all the stable isotopes in the periodic table. We propose to measure the temperature increase of the wire containing gadolinium isotopes, which occurs when neutrons penetrate the wire and deposit some energy into the wire.

2.9. Experiments on the diagnostics of beams using vibrating wire monitors

Electron beams

The first experiments on scanning charged particle beams were carried out on the electron beam of the Yerevan Physics Institute synchrotron injector with energy of 50 MeV and an average current of about 10 nA after collimation [34]. A monitor with a large aperture formed by a 50 mm long target wire was also used to measure the electron beam profile (see[1]).

[1] Arutunian S.G., Avetisyan A.E., Davtyan M.M., Vasiniuk I.E., Yerevan synchrotron injector electron beam transversal scan with vibrating wire scanner, Izv. AN Armenii, Fizika, 2011, pp. 389-397.

Proton beams

A series of experiments on the use of VWM was carried out at the PETRA accelerator at DESY when PETRA served as a proton booster for HERA. The unique characteristics of the VWM made it possible to measure the halo region of the proton beam with an average current of about 15 mA and energy of 15 GeV [35, 36].

A monitor with an expanded aperture of 60 mm with a total wire length of 120 mm was installed on the transport line between the linear accelerator and the 3 GeV synchrotron of the J-PARC complex. The ability of the monitor to diagnose a halo beam was confirmed. As a positive characteristic, the sensor was insensitive to secondary electrons [37]. The extended aperture of the VWM is planned to be used to study the proton beam halo of the Project-X Injector (PXIE, Fermilab), which is a program aimed at developing a multimegawatt superconducting proton accelerator. The VWM was tested on a Fermilab High Intensity Neutrino Source (HINS) setup with a 50 keV proton beam [38, 39].

Ion beams

A VWM was tested on a beam of iron ions with energy of 20 keV and a current of 16 pA of the EMAL-2 energy-mass analyzer. A frequency shift at a level of 0.15 Hz was registered (see[1]).

Diagnosis of photon beams: Laser beams

Usually laser beams, as the most accessible for experiments, were used in the process of developing and calibrating vibrating wire monitors of all types. As a rule, conventional semiconductor lasers with power from few to several hundred mW are used.

The resonance target method (RT-VWM) has so far been tested only on a semiconductor laser beam. Fast photodiodes were used as detectors of reflected

[1] Arutunian S.G., Bakshetyan K.G., Dobrovolski N.M., Mayilyan M.R., Oganessian V.A., Soghoyan A.E., Vasiniuk I.E., Wittenburg K., Vibrating wire scanner parameters optimization Proc. 9-th Europ. Part. Accel. Conf., Lucerne, Switzerland, 5-9 July 2004, pp. 2457-2459.

radiation [40]. The laser beam profiling area, however, may have an independent interest[1].

X-ray (undulator) radiation

Despite the fact that this radiation only deposits a small part of its energy in the wire, due to the high sensitivity of the vibrating wire monitors, this energy was enough to heat the vibrating wire at the level of the frequency shift resolution. Experiments were performed at APS ANL (Advanced Photon Source of Argon National Laboratory) to measure the X-ray profile from an undulator with an energy range of 6.5–19.5 keV and the size of an unfocused beam of 3 × 1.5 mm. Important in the task was the emission of radiation only from this device with suppression of the background by softer synchrotron radiation photons, generated when the electrons passed the magnetic fields of the focusing and deflecting magnets. Such a suppression was made by a beryllium filter plate. As a result, only the x-ray emission of the undulator remained after the filter, which was measured by the VWM [41].

Synchrotron radiation

At the APS ANL synchrotron, an experiment was carried out to measure the parameters of the electron beam using the SI. It is important that such a measurement was carried out outside the vacuum chamber behind the copper flange of one of the unused SI channels. In general, radiation with a power of about 99.1 W with a peak near 10 keV was absorbed in a 6 mm thick copper flange, and only hard photons with an energy of more than 100 keV (SR spectrum tail) with a power of 420 mW passed through the flange. About 1.1 mW of power converted to heat was deposited on the wire. The electron beam of the synchrotron, by means of the magnetic optics of the accelerator, was scanned in an angle within the limits of 300 μrad with a step of 2.4 μrad. As a result, the fixed five-wires vibrating wire monitor installed behind the flange provided five SI profiles representing the electron beam profile.

---

[1] Aginian M.A., Arutunian S.G., Hovhannisyan V.A., Mailian M.R., Wittenburg K., Vibrating wire scanner/monitor for photon beams with wide range of spectrum and intensity.- NATO Advanced Research Workshop “Advanced Photon Sources and Their Application” Nor Amberd, Armenia, August 29 - September 02, 2004.

2.10. Conclusion

In the present practical course, we collected information on a wide range of traditional methods of beam profile measurements and described in details the method based on a vibrating wire. The operation principle of the vibrating wire monitor (VWM) is based on a simple and clear idea of the frequency dependence of a mechanical resonator (stretched wire) on the wire tension. The wire tension, in turn, depends on its temperature, i.e. the instrument is essentially a precise thermometer with the range of temperature shifts from mK to few hundreds of K.

The main advantage of the method is its high sensitivity to the local flux of particles penetrating the wire and the wide dynamic range. That makes the method also a precise instrument for halo measurement of a beam with stable characteristics. This requirement arises from the large response time of the VWM that is the main disadvantage of the method. The instrument is very compact and consists practically of a simple resonator and a small scheme of vibration excitation. The operation principle is very clear and demonstrable. Due to the thermal principle of operation, a VWM can be used for any type of heat deposited by a beam into the wire (charged particles, electromagnetic radiation in wide spectral range, neutrons).

Students will perform the following practical work items:

- Familiarization with VWM operation principle of vibrating wire sensors/monitors.
- Choice of wire tension corresponding to the given VWM parameters.
- Check proper generation by oscilloscope.
- Wiring of VWM test bench.
- Run the application program (digital oscilloscope) of wire frequency measurement.
- Prepare laser beam profile measurement by means of VWM.
- Measurement the VWM frequency signal at forward and backward scan using the application program.

- Familiarization with electron beam profile measurement by means of VWM.
- Check the communication lines between accelerator area and control room.
- Acquire the data from scan station equipped with VWM by corresponding application program.
- Compare results with beam profile measurement by of YAG:Ce crystal station for AREAL beam profile measurement (see[1])

We hope that the proposed course will help students to quickly master the attainments of beam profiling using vibrating wire monitors, and based on the obtained skills get ready for using other existing methods in their further work.

A detailed description of the practical work done by students is given in a separate manual[2].

2.11. References

[1]. P. Forck, Lecture Notes on Beam Instrumentation and Diagnostics, Gesellschaft fur Schwerionenforschung (GSI) Darmstadt, Germany,Joint University Accelerator School, January – March 2011, pp. 143. URL: https://www-bd.gsi.de/conf/juas/juas_script.pdf.

[2] E. Bravin. Transverse Beam Profiles - 2008. in Proc. CERN Accelerator School on Beam Diagnostics (CAS'08), Dourdan, France, pp. 377-406.

[3] K. Wittenburg, Specific instrumentation and diagnostics for high -intensity hadron beams, DESY, Hamburg, Germany, arXiv:1303.6767 [physics.acc-ph], 2013.

[4] P. Strehl, Beam Instrumentation and Diagnostics, Springer-Verlag, Berlin, Heidelberg, 2006.

[5] D. Brandt, CAS CERN Accelerator School Beam Diagnostics, Dourdan, France 17 August 2009, p. 597.

[6] S. Burger C. Carli, M. Ludwig, K Priestnall, U. Raich, THE PS BOOSTER FAST WIRE SCANNER, Proc. Diagn. Instrum Part Acc. Conf. DIPAC03, Mainz, 2003, p. 122-124.

[1] Joint German–Armenian Student Practical Course on Accelerator Physics, Armen Grigoryan, Artsrun Sargsyan, Gevorg Zanyan, Vahe Sahakyan, Gayane Amatuni, PracticalCourses_BeamDiagnostics.docx, CANDLE, 2019.
[2] Hands-on lab steps of practical course: Vibrating wire monitors and beam profile measurements.

[7] D. M. Harryman, C. C. Wilcox, An upgraded scanning wire beam profile monitoring System for the ISIS high energy drift space, 6th International Beam Instrumentation Conference, IBIC2017, Grand Rapids, 2017, pp 396-400

[8] P. Dirksen, M. Lenckowski, W.R. Rawnsley, M. Rowe, V. Verzilov, A Fast Wire Scanner for the TRIUMF Electron Linac, 6th International Beam Instrumentation Conference, IBIC2017, Grand Rapids, 2017, pp.401-403.

[9] M. Veronese, S. Grulja, G. Penco, M. Ferianis, S. Dal Zilio, S. Greco1, M. Lazzarino, L. Fröhlich, A NANOFABRICATED WIRESCANNER: DESIGN, FABRICATION AND EXPERIMENTAL RESULTS, 6th International Beam Instrumentation Conference, IBIC2017, Grand Rapids, MI, USA, 2017, pp. 314-317.

[8] S. Borrelli, M. Bednarzik, C. David, E. Ferrari, A. Gobbo, V. A. Guzenko, N. Hiller, R. Ischebeck, G.L. Orlandi, C. Ozkan-Loch, B. Rippstein and V. Schlott., Wire Scanner on a Chip, URL: http://accelconf.web.cern.ch/AccelConf/ibic2017/talks/we2ab2_talk.pdf

[10] G. F. Knoll, Radiation Detection and Measurement, John Willey, New York (1999).

[11] V. Mihailov et al., General-purpose ionization detectors for accelerated particle beams, Instr. and Exp. Tech. 6 (1995) 39.

[12] S. Gavrilov, P. Reinhardt-Nickoulin, A. Titov, 2d non-destructive transverse diagnostics by beam cross-section monitors, 6th International Beam Instrumentation Conference IBIC2017, Ljubljana, Slovenia, 2017, pp 393-395.

[13] Y. Hashimoto, Y. Fujita, T. Morimoto, S. Muto, T. Fujisawa, T. Honma, K. Noda, Y. Sato, S. Yamada, Chiba, Japan H. Kawauchi, A. Morinaga, Y. Taki, K. Takano, J. Takano, DEVELOPMENT OF A NON-DESTRUCTIVE BEAM PROFILE MONITOR USING A GAS SHEET, Proc. Part. Acc. Conf. PAC2001, Chicago, 2001, pp. 1631-1633.

[14] H. Koziol, BEAM DIAGNOSTICS FOR ACCELERATORS, CERN, Geneva, Swizterland, URL: http://www.isa.au.dk/accfys/E08/Download/Koziol_BeamDiagnostics.pdf.

[15] D. Vilsmeier, Space-charge distortion of transverse profiles measured by electron-based ionization profile monitors and correction methods, PHYSICAL REVIEW ACCELERATORS AND BEAMS 22, 052801 (2019).

[16] G. Kube, Particle beam diagnostics and control, URL: https://bib-pubdb1.desy.de/record/91024/files/KubeLecture.pdf.

[17] T. F. da Silva, Beam monitoring using Optical Transition Radiation, URL: http://beamdocs.fnal.gov/AD/DocDB/0036/003631/002/Chicago%20Presentation.pdf

[18] M. Turner et al., Experimental Observation of Plasma Wakefield Growth Driven by the Seeded Self-Modulation of a Proton Bunch, PHYSICAL REVIEW LETTERS 122, 054801 (2019).

[19] E.J. Jaeschke, S. Khan, J.R. Schneider, J.B. Hastings, Synchrotron Light Sources and Free-Electron Lasers, Accelerator Physics, Instrumentation and Science Applications, Springer International Publishing Switzerland 2016.

[20] B. Li, H. Hao, J.-Y. Li, Y. K. Wu, Transverse beam profile measurement system for the Duke storage ring, Nuclear Inst. and Methods in Physics Research, A, Volume 911, p. 45-50.

[21] K. TANG, B.-G. SUN, Y.-L. YANG, P. LU, L.-L. TANG, F.-F.WU, C.-C. CHENG, J.-J. ZHENG, H. LI, Transverse beam size measurement system using visible synchrotron radiation at HLS, arXiv:1602.07918v1 25 Feb 2016, p.1-8.

[22] L. Torino and U. Iriso, Transverse beam profile reconstruction using synchrotron radiation interferometry, PHYSICAL REVIEW ACCELERATORS AND BEAMS19,122801 (2016).

[23] D.M. Stefanescu, Handbook of force transducers: principles and components, Berlin : Springer-Verlag, 2011.

[24] A.J. Simmonds, Long term monitoring using vibrating wire sensors, Geokon Inc., Lebanon, NH, USA, 2015.

[25] Arutunian S.G. Dobrovolski N.M.,. Mailian M.R, Sinenko I.G., and Vasiniuk I.E., Vibrating wire for beam profile scanning, Phys. Rev. Special Topics - Accelerators and Beams, 1999, v. 2, 122801.

[26] Arutunian S.G. Vibrating wire sensors for beam instrumentation, Beam Instrumentation Workshop, BIW08, (May 4-8, 2008, Lake Tahoe, USA), pp. 1-7.

[27] S.G. Arutunian, J.Bergoz, M.Chung, G.S.Harutyunyan, E.G.Lazareva, Thermal neutron flux monitors based on vibrating wire, NIM A, 797, 37-43 (2015).

[28] W.R. Leo. Techniques for Nuclear and Particle Physics Experiments. New York, Berlin, Heidelberg, Springer-Verlag, 1987.

[29] K.A. Olive et al. PASSAGE OF PARTICLES THROUGH MATTER, Chin. Phys. C, 38, 090001 (2014) and 2015 update.

[30] I. Wingerter-Seez, Particle physics instrumentation, arXiv:1804.11246v1 physics.ins-det] 30 Apr 2018.

[31] G. Budker, Proc. 7th Int. Conf. High-Energy Accel., Yerevan, 1970, p. 33. Yerevan: Publ. House Acad. Sci. Armen. SSR (1970).

[32] M.A. Palmer, S. Brice, A.D. Bross, D. Denisov, E. Eichten, R. Lipton, D.V.Neuffer, H. Kirk, R. Palmer, M.Kaplan, P. Snopok, A. Bogacz, C. Ankenbrandt, J-P. Delahaye, P. Huber, MUON ACCELERATORS FOR THE NEXT GENERATION OF HIGH ENERGY PHYSICS EXPERIMENTS, Proc. IPAC2013, Shanghai, China, 2013, pp. 1475-1477.

[33] S.G. Arutunian, J.Bergoz, M.Chung, G.S.Harutyunyan, E.G.Lazareva, Thermal neutron flux monitors based on vibrating wire, Nuclear Instruments and Methods in Physics Research A 797, 2015, pp. 37-43.

[34] Arutunian S.G., Dobrovolski N.M., Mailian M.R., Vasiniuk I.E., Vibrating wire scanner: first experimental results on the injector beam of Yerevan synchrotron.- Phys. Rev. Special Topics, Accelerators and Beams, 2003, v. 6, p. 042801.

[35] Arutunian S.G., Mailian M.R., Wittenburg Kay, Vibrating wires for beam diagnostics, Nucl. Instrum. Methods A, 572, 2007, pp 1022-1032.

[36] Arutunian S.G., Werner M., Wittenburg K. Beam tail measurements by wire scanners at DESY - ICFA Advanced Beam Dynamic Workshop: Beam HALO Dynamics, Diagnostics, and Collimation (HALO`03) (in conjunction with 3rd workshop on Beam-beam Interaction), Gurney`s Inn, Montauk, N.Y. USA, May 19-23, 2003.]

[37] K. Okabe, M. Yoshimoto, K. Yamamoto and M. Kinsho, A preliminary study of the vibration wire monitor for beam halo diagnostic in J-PARC L3BT, Proceedings of IPAC2013, Shanghai, China, 2013, pp. 535-537.

[38] M. Chung, V. Scarpine, B. Hanna, J. Steimel, V. Shiltsev, S.G. Arutunian, S. Artinian, Transverse beam halo measurements at high intensity neutrino source (hins) using vibrating wire method, Proc. of IPAC2013, Shanghai, China, 2013, pp. 819-821

[39] S.G. Arutunian, A.E. Avetisyan, M.M. Davtyan, G.S. Harutyunyan, and I.E. Vasiniuk, M.Chung, V.Scarpine, Large aperture vibrating wire monitor with two mechanically coupled wires for beam halo measurements, Physical Review Special Topics - Accelerators And Beams, 2014, Vol 17, 3, pp. 032802-1...11.

[40] Arutunian S.G., Margaryan A.V., Oscillating wire as a “Resonant Target” for beam transversal gradient investigation, proceedings of IPAC2014, ISBN 978-3-95450-132-8, Dresden, Germany, 2014, pp. 3412-3414.

[41] G.Decker, S.Arutunian, M.Mailian, G.Rosenbaum, First vibrating wire monitor measurements of a hard x-ray undulator beam at the Advanced Photon Source, DIPAC 2007, Venice, Italy, pp. 36-38